DOI:10.14753/SE.2025.3208

SEMMELWEIS EGYETEM

DOKTORI ISKOLA

Ph.D. értekezések

3208.

HAJNAL BOGLÁRKA ZSÓFIA

Klinikai neurológiai kutatások

című program

Programvezető: Dr. Kovács Tibor, egyetemi tanár

Témavezető: Dr. Fabó Dániel, egyetemi adjunktus

DOI:10.14753/SE.2025.3208

EVALUATION OF SPONTANEOUS AND ELECTRICALLY EVOKED ELECTROPHYSIOLOGICAL PHENOMENA IN EPILEPTIC PATIENTS IMPLANTED WITH LAMINAR MICROELECTRODES

PhD thesis

Boglárka Zsófia Hajnal, MD

Semmelweis University Doctoral School

János Szentágothai Neuroscience Division

Supervisor: Dániel Fabó, MD, Ph.D.

Official reviewers: Szilvia Gulyás, MD, Ph.D.
Domokos Meszéna, Ph.D.

Head of the Complex Examination Committee: Dániel Bereczki, MD, D.Sc.

Members of the Complex Examination Committee: Melinda Lukács, MD, Ph.D.
Gábor Csukly, MD, Ph.D.

Budapest
2025

DOI:10.14753/SE.2025.3208

Table of Contents

DOI:10.14753/SE.2025.3208

DOI:10.14753/SE.2025.3208

List of Abbreviations

AS: amplitude spectrum
CCEP: Cortico-cortical evoked potential
CSD: Current source density
CT: Computed tomography
ECoG: Electrocorticography
EEG: Electroencephalogram
ERSP: Event-related spectral perturbation
fMRI: functional MRI
IAM: Individual Adjustment Method
IID: interictal discharge
LFP: Local field potential
LFPg: Local field potential gradient
LME: Laminar microelectrode
LTP: Long-term potentiation
MRI: Magnetic resonance imaging
MUA: Multiple unit activity
NREM: Non-rapid eye movement
PCA: principal component analysis
PET-MRI: positron emission tomography-MRI
SOZ: seizure onset zone
SPES: Single-pulse electric stimulation
SUA: Single-unit activity
SW: Slow wave
sSW: Spontaneous SW
SWd: SW downstate
TFR: Time–frequency representation
TMS: Transcranial magnetic stimulation
TRN: thalamic reticular nucleus

DOI:10.14753/SE.2025.3208

I. Introduction

I.1. Evaluation of epileptic patients with invasive electrodes

Epilepsy surgery offers a potential cure for patients with drug-resistant epilepsy. In the case of resective surgery, the success of the procedure depends on the accurate identification of the seizure onset zone (SOZ) during preoperative assessment. In cases where the results of preoperative non-invasive investigations (MRI, fMRI, PET-MRI, neuropsychological tests, scalp EEG, seizure symptoms) do not allow a clear localization of the seizure onset zone due to discordant data or in cases where a deep or eloquent area close focus is suspected, further examinations with invasive electrodes (subdural grid (1), strip (2), or stereo-EEG (3)) may be necessary. These surgically implanted subdural or deep brain electrode systems can not only be used to study the pathophysiology of epilepsy, but also offer a unique opportunity to study physiological brain oscillations. In addition to the electrodes routinely used in clinical practice, we used a special intracortical laminar microelectrode (LME) system (4) to study local neocortical pathological and physiological changes. Previously, our group has investigated the local cortical mechanisms of interictal epileptiform discharges (5), high-frequency oscillations (6), sleep slow waves (7) and K-complex (8) generation. In our current study we focused on the laminar analysis of sleep spindles (9) and electrically evoked cortical potentials (CCEPs) (10). Additionally, we sought to demonstrate that the intracortical characteristics of electrically evoked surface negativities during wakefulness resemble those of spontaneous slow wave (SW) downstates during sleep (10).

I.2. Sleep spindles

Sleep spindles are approximately sinusoidal oscillations generated by interactions between thalamocortical, corticothalamic, and reticular thalamic networks (11-13). They are observable on both scalp EEG and ECoG recordings (14). These spindles are characterized by neural firing patterns that promote long-term synaptic changes, including long-term potentiation (LTP) (13). Sleep spindles have been widely studied for their role in memory functions and sleep regulation (12, 15). They are linked to learning efficiency (16, 17) and general cognitive ability (18) and serve as important clinical markers in various neurological and psychiatric conditions (19-23). Given that sleep

spindles originate in thalamocortical networks, they are influenced by the anatomical structure of thalamocortical connections. Based on the distinction between 'core' and 'matrix' thalamocortical pathways (24, 25) – which target cortical layer IV and layers I-II, respectively – it has been suggested that sleep spindles may arise from either or both networks, with potentially varying contributions from each (26). As different thalamocortical projections reach different cortical layers, the thalamic source of EEG events can be inferred from the current source density patterns recorded from electrodes that penetrate the cerebral cortex (4, 27). Studies in epileptic patients have mapped the laminar profile of the K-complex (8) and the slow wave (7), both of which predominantly originate in superficial layers. Research in animals (28, 29) – though not explicitly framed within the core-matrix model – has shown that various thalamocortical networks contribute to spindle generation, with a prominent sink in layer IV and an additional, more superficial sink. Recent research using laminar probes in epileptic subjects (30) found that cortical spindles occur with diverse topographies, with some localized to either upper or middle cortical layers. Sleep spindles differ in at least two characteristics which may be associated with a different network of origin, and consequently a different laminar profile. First, sleep spindles can be divided into functionally different slow and fast subtypes, based on their frequencies (12, 14). Second, there is substantial variability in the spatial extent (globality) of spindles (14, 31, 32). Although, the division of sleep spindles based on their extent- i.e. local versus global spindles- is arbitrary, because it depends largely on the number of sampling points, i.e. the detection technique. There is some evidence on how thalamocortical spindle generators differ between slow and fast spindles or spindles with varying cortical involvement. First, an in-silico simulation of thalamocortical networks (33) suggested that wider thalamocortical connections to superficial layers promote greater spatial extent and cortical synchrony of spindles. Second, pharmacological studies show differential effects on slow and fast spindles: the Ca2+ channel antagonist flunarizine selectively reduces fast spindle activity, while the Na+ channel antagonist carbamazepine reduces fast spindle activity but increases slow spindle and ~0.75 Hz slow wave activity (34). Ca2+ channels, particularly in the reticular nucleus (TRN), are key in thalamic spindle generation (13, 35), and the resilience of slow spindles to Ca2+ channel blockade suggests that they may be generated independently of the thalamus, challenging traditional theories of spindle generation (36). It has also been

hypothesized that slow and global spindles rely more on thalamocortical or possibly cortico-cortical networks terminating in superficial layers ("matrix" network), whereas fast and local spindles depend on the more focused "core" network (26). Accordingly, slow, and global spindles would be associated with more superficial activations, while fast and local spindles would activate deeper cortical layers. Recent findings show that spindle-frequency oscillations in the cortical depths display a heterogeneous topography (30), though the relationship between spindle topographies and subtypes remains unclear (9).

I.3. Cortical potentials evoked by single pulse electrical stimulation

Single-pulse electrical stimulation (SPES) is commonly used in presurgical evaluation of epileptic patients with implanted intracranial electrodes. Cortico-cortical evoked potentials (CCEPs), especially those evoked by low-frequency (≤1Hz) SPES, help map brain network organization (37) and can assist in locating pathological areas (38, 39). CCEPs refer to a consistent series of early physiological responses, while later deflections (>100ms) with varied latencies, such as repetitive or delayed responses and afterdischarges (40), are considered pathological (41). However, this distinction is debated, as late components can also appear under normal conditions, and early components may be influenced by pathological processes (42, 43). Changes in early CCEP responses can indicate reorganization within epileptic networks (44, 45). Typically, CCEPs include an early negative component (N1: 10-50ms) linked to direct cortico-cortical projections within functional networks, and a later negative component (N2: 50-500ms), which involves both cortico-cortical and cortico-subcortico-cortical circuits, representing intra- and internetwork connections (46-49). Additionally, smaller positive components, P1 (before N1) and P2 (following N1), have been noted (50). In our study, we identified a further late positive potential, termed P3 (10). Despite the widespread use of cortical stimulation, the intracortical mechanisms underlying CCEP generation in humans remain unknown (10).

I.4. Spontaneously occurring and evoked sleep slow waves

A slow wave (SW) is defined by alternating cortical up and down states during NREM sleep stage 3 (51), and it has been widely studied in both cats (52) and humans (53, 54). The active phase (up-state), marked by membrane depolarization, involves excitatory and inhibitory postsynaptic potentials, while the inactive phase (down-state), marked by hyperpolarization, reflects a global disfacilitation in the cortico-thalamic network (52). Animal studies have shown that both cortico-cortical and cortico-thalamic networks contribute to SW generation (52), but the mechanisms are less understood in humans. Though cortical networks alone can produce SWs—demonstrated in thalamectomized cats (52) and cortical slice preparations (55)—the thalamus is crucial for synchronizing cortical neuron populations (56). Research on animals suggests that SWs can originate in any cortical layer, most commonly in infragranular layers, with layer V pyramidal cells playing a key role in up-state initiation (55, 57). However, studies in anesthetized rats with spinal cord injury show increased SW initiation in layer II/III (58). Interestingly, Csercsa et al. observed the generation of SWs detected in epileptic patients primarily in supragranular layers (7). Whether these differences are due to pathological reorganization of the epileptic neocortex or interspecies variations in cortical cell population, remains unclear (59). SWs appear over large cortical areas due to local intracortical connections (60) and travel from one definite region to all over the scalp mostly within the default mode network (54, 61). Nevertheless, SWs can also remain local, associated with local cessation of neuronal firing (62). SWs can be elicited during sleep by cortical stimulation using transcranial electric (63), -magnetic stimulation (TMS) (64, 65) in humans, and by intracortical electrical stimulation in rats (66). Spontaneous, local, sleep-like cortical phenomena have been observed at the regional or columnar level in awake rats under sleep pressure (66) and in human participants (67). In humans, these phenomena have also been associated with attentional lapses even without sleep deprivation (68, 69), suggesting that local sleep states can coexist with wakeful brain activity. However, there is limited and somewhat contradictory evidence on whether and how SWs can be induced in the awake state (64, 70). Massimini et al. (64) reported being unable to evoke SWs in awake individuals (10).

DOI:10.14753/SE.2025.3208

II. Objectives

By examining both sleep spindles and cortico-cortical evoked potentials (CCEPs), using simultaneous electrocorticographic (ECoG) and laminar (LME) recordings in humans, our aim was to extend prior work on cortical layering to provide a more detailed picture of laminar functionality in both spontaneous and evoked cortical processes.

My main hypotheses are:

1. Different types of sleep spindles (slow/fast, local/global) are generated by different thalamo-cortical networks.
2. Single pulse electrical stimulation of the neocortex triggers a specific excitatory-inhibitory sequential proccess, with various involvement of different cortical layers.
3. The underlying mechanisms of late components of CCEPs are similar to those observed during sleep slow wave down- and upstates, i.e. a local sleep-like phenomenon can be evoked by electrical stimulus in the awake state.

In the present work I aimed to investigate how neural networks associated with different cortical layers contribute to the generation of sleep spindles and whether this contribution varies across spindle types (slow/fast, local/global). To prove our hypotheses, we examined the cortical profiles (using LFP, CSD, MUA and SUA analyses) of “micro-domain” (LME) and “macro-domain” (ECoG) spindles to assess their dependence on sleep spindle type. In addition, we analyzed the intracortical profile of various CCEP components to understand the function of local cortical circuits during cortical electrical stimulation. Based on the results of these analyses, we aimed to propose a hypothetical model to describe intracortical activation and inhibition during cortical electrical stimulation. To prove our hypothesis that the late components of the CCEPs correspond to a sleep slow wave, we compared in detail the cortical presentation patterns of the two phenomena.

DOI:10.14753/SE.2025.3208

III. Methods

III.1. Patient selection

Seven patients with focal epilepsy (4 males, average age 25.42 ± 11.37 years), undergoing phase 2 presurgical evaluation in our institute (Department of Neurosurgery and Neurointervention, Semmelweis University, Budapest, Hungary) were included in the evoked potential part of the study. Detailed patient characteristics are provided in Table 1. Informed consent was obtained from all participants or their legal guardians in line with the Declaration of Helsinki, and the study received approval from the National Scientific and Ethical Committee of the Medical Research Council in Hungary (approval numbers: 242/KO/2001 6008/6/2001/ETT and 20680-4/2012/EKU (368/PI/2012)). The paradigm of cortical stimulation was related to current study and was included in the ethical approval. For the sleep spindle analysis, electrophysiological data were selected from four of the seven patients whose NREM sleep phase could have been clearly identified based on EEG and the signal quality of both ECoG and LME data was adequate for spindle analysis (Table 1, yellow-colored columns) (9, 10).

III.2. Electrode implantation and reconstruction

All patients underwent fluoroscopy aided subdural strip and grid implantation (AD TECH Medical Instrument Corp., Racine, WI, USA: various subdural electrodes) planned entirely on clinical grounds. Up to two LMEs (24 contact, 150μm intercontact distance, 3.5mm span; Neuronelektród Ltd., Budaörs, Hungary, Fig.1f) were inserted perpendicular to the cortical surface underneath the subdural electrodes for scientific purposes (4, 8, 71) (Fig. 1a-d). Following electrode implantation, the surface electrode and LME locations were superimposed on the 3D reconstructions of preoperative MRIs based on postoperative CT scans (Fig. 1e). A gyrus likely to be removed later was selected for microelectrode implantation. After securing the output leads of the LME with appropriate stitches, the subdural grid electrode was positioned above the multielectrode. The electrode penetration track was reconstructed upon removal in the surgical block(7, 72, 73) (Fig. 1a-d). Surgery was performed in six out of seven cases. The electrode containing tissue block was removed in 4 patients (Pt.1, 2, 3, 5; Table1/CCEP study). The resected

DOI:10.14753/SE.2025.3208

tissue was cut into 2–5 mm blocks and chemically fixated (7, 73). The laminar topography of the cortical tissue blocks was reconstructed from these samples and it was used to determine the location of LME electrodes within cortical layers, taking into account the shrinkage of brain tissue during preparation (7, 74). The cortical layer from which an LME signal originated was estimated based on the histological reconstruction of the electrode track (9, 10).

Table 1. Summary of patients involved in the spindle and CCEP studies (9, 10). The numbers in parentheses indicate the number of the multielectrode selected for analysis in cases where two electrodes have been implanted. *Pt* patient, *F* female, *M* male, *R* right, *y* year, *gy* gyrus. Note that only 4 out of 7 patients were selected for the spindle study.

spindle study	CCEP study	Gender	MRI finding	Age at surgery	LME location	Seizure type	Distance between stimulated and recording electrodes (CCEP study)	slow spindle frequency range	fast spindle frequency range	Number of sleep spindles			
										$N_{slow,\ global}$	$N_{slow,\ local}$	$N_{fast,\ global}$	$N_{fast,\ local}$
Pt1	**Pt1**	F	normal	34 y	R frontal (Th2)	Focal, tonic postural	2.5 cm	11.45-12.61	13.3-14.67	73	19	76	19
Pt4	**Pt2**	M	R fronto-centro-opercular dysgenesis	20 y	R frontal	Focal, hypermotor	1 cm	11.28-12.22	13.49-14.44	404	167	324	241
Pt2	**Pt3**	M	R frontal dysgenesis	16 y	R frontal (Th2)	Focal, tonic postural	1.5 cm	10.43-11.54	12.49-13.38	335	256	460	356
	Pt4	F	R frontal dysgenesis	19 y	R frontal	Focal, tonic postural	<1 cm						
Pt3	**Pt5**	M	R parietal dysgenesis	13 y	R frontal	Focal sensory-motor hemiconvulsive	2.5 cm	12.26-13.5	13.64-15.28	34	97	28	84
	Pt6	F	R frontal-cingular dysgenesis	44 y	R frontal (Th2)	Multifocal	1.5 cm						
	Pt7	M	R inferior frontal gy. dysplasia	32 y	R frontal (Th1)	Focal, hypermotor	1 cm						

DOI:10.14753/SE.2025.3208

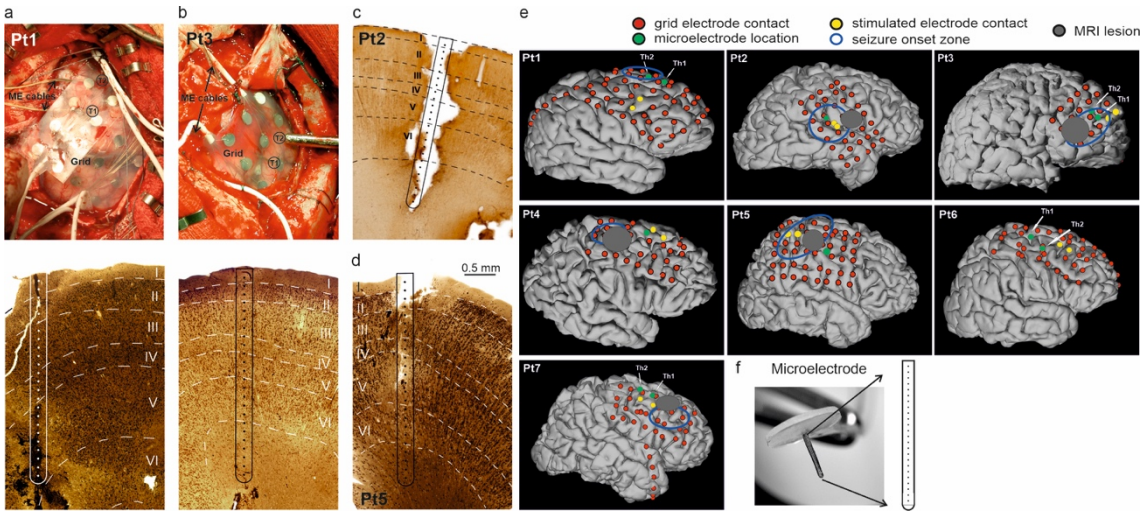

Figure 1. Macro- and microelectrodes (10). *(a, b row 1)* Intraoperative photo showing a surface subdural grid electrode and two "thumbtack" multielectrodes (T1 and T2) for LFP and SUA recordings in Pt1 and Pt3. *(a, b row 2, c, d)* Histological reconstruction of electrode tracks showing cortical lamination around microelectrodes in Pt1, Pt2, Pt3, and Pt5. Note that all the histologically evaluated electrode tracks verified normal cortical lamination around the electrode trajectory. *(e)* 3D MRI reconstructions with electrode locations for seven patients, showing surface electrodes (grid and strip; red filled circle), microelectrode (green filled circle), and stimulated electrode contacts with best-response (yellow filled circle) relative to seizure onset zones (blue open circle) and MRI lesions (grey filled circle). Laminar electrodes were placed outside MRI lesions but near seizure onset zones. *(f)* Photo of a 24-contact laminar microelectrode.

III.3. Surface and laminar recordings

Following implantation, patients were admitted to the epilepsy monitoring unit and continuously monitored for epileptic activity. Video-EEG monitoring was carried out using a standard hospital system (Brain Quick System 2 or 98 or Plus Evolution, Micromed, Mogliano Veneto, Italy). All signals were recorded with mastoid reference (Acquisition rate: 1 or 2 kHz/channel, 16 bit, no filtering) and stored on external hard disks for offline analysis. The data obtained from LMEs were recorded by a separate system consisting of a custom-built preamplifier, amplifier, and a Labview-based acquisition software (National Instruments, Austin, TX), allowing recording of the gradient local field potential (LFP) as a voltage difference between two adjacent electrode

contacts. LFP (0.1–500 Hz, 2 kHz/channel, 16 bit) and multiple unit activity (MUA) (500–5000 Hz, 20 kHz/channel, 12 bit) were recorded from the LMEs simultaneously while the patients were awake or sleeping (4). LME recordings were co-registered to the surface ECoG recordings using a common marker generated by an external trigger computer (9, 10).

III.4. Detection and analysis of sleep slow waves and sleep spindles

The sleep staging was performed by an expert neurophysiologist (D.F.) based on scalp-EEG and ECoG. The downstate phases of SWs were then detected visually on the corresponding laminar recordings of NREM sleep stage 3. Layer II signal was filtered (low pass 5 Hz, 24 dB/oct, zero-phase shift). Next, exact downstate positions were refined as local minima of the filtered signal. Two second-length epochs (± 1000 ms) time-locked to downstate peaks and averaged for each LME channel were used for spectral, current source density (CSD) and MUA analyses (see sections below).

For spindle analysis, the hypnograms were visually scored for ECoG data on a 20 second basis using standard criteria (75). Artifact-free NREM stage II and III data underwent sleep spindle detection using the Individual Adjustment Method (IAM) (76, 77), identifying slow and fast spindle frequencies for each subject. The IAM essentially defines sleep spindles as waveforms with a specific frequency and sufficient amplitude that contributes to the spectral peaks of the NREM sleep EEG. In the first step, the high-resolution (0.0625 Hz) amplitude spectrum (AS) of the visually scored, artifact-free NREM sleep EEG was calculated for each ECoG channel free of interictal discharges (IIDs, “spikes”) based on 4 sec segments (Hanning-tapered, zero padded to 16 sec to ensure sufficient resolution in the frequency domain). A spectral peak was defined as the interval within which second-order AS derivatives were below zero. In line with the assumptions of the IAM about the spectral characteristics of sleep spindles, two clear spectral peaks were visible for each subject, one for slow spindles and another for fast spindles. In the second step, ECoG data was filtered to the subject’s individual slow or fast sleep spindle frequency range, and sleep spindles were identified as events in which the amplitude exceeded an electrode-specific threshold defined as the average of the AS values at the spectral peak boundaries, multiplied by the number of high-resolution

frequency bins within the frequency range. If this dynamically defined threshold was not exceeded for at least 0.5 second, no sleep spindle was detected. Sleep spindles were detected in this manner for IID-free ECoG channels and LME channels with no permanent artifacts. An ECoG spindle was considered as “local” if it was detected in less than or equal to 33% of the IID-free ECoG channels, and “global” if it occurred in more than 33% of IID-free ECoG channels. The exact timing of ECoG sleep spindles were defined on the channel spatially closest to the LME for the analysis of laminar dynamics. ECoG data from this channel was filtered to the individual slow and fast spindle frequency, respectively, as it was determined in the first step of the IAM (two-way FIR filtering). LME data was triggered to the maximum positive deflection of the spindle cycle closest to the point where the envelope (defined as the modulus of the Hilbert transform of the filtered signal) of the filtered signal of this spatially closest ECoG electrode was maximal (spindle peak). LME LFPg data segments from -500 msec to 500 msec relative to the identified ECoG spindle peaks were selected for further analysis. All data segments were filtered to a generic sleep spindle range (10-16 Hz, two-way FIR filtering implemented in Matlab EEGLab) and smoothed across layers using a Hamming window. For further analysis steps on CSD, MUA and SUA analysis, see the section below. EEG analysis was performed using Fercio© (Ferenc Gombos, Budapest, Hungary) for the IAM analysis, MATLAB 2018b (The MathWorks, Inc., Natick, MA) EEGLab (Swartz Center for Computational Neuroscience, San Diego, CA) for filtering, envelope calculation and data synchronization (9).

III.5. Single pulse electrical stimulation (SPES) of the neocortex

Cortical stimulation was performed at the bedside on post-implant day 3 to 7. In all cases, before the electrical stimulation sessions, we have already had recorded enough spontaneous seizures for clinical analysis. Stimulation was performed in seizure free periods, at least 4 h after the last recorded seizure. All patients underwent stimulation in the awake state (alert state with eyes opened), verified by video observations and EEG patterns. SPES (bipolar, 10 mA, 0.5 Hz, biphasic, square pulse, pulse width: 0.2 ms, trial: 20–150) was administered to each adjacent pair of grid and strip electrodes using IRES Surgical 600 stimulator (Micromed S.p.A. Via Giotto, 2-31021, Mogliano Veneto—Italy) (Pt 1, 3, 5) or built in Micromed stimulator from 2015 (Pt. 2, 4, 6, 7). The number of

stimuli per pair of electrodes varied from 25 to 150, depending on the patient's clinical state (stimulation was interrupted if the patient had a seizure during the protocol) and clinical question (considering the relevance of eliciting abnormal CCEPs in presurgical planning). All patients had one stimulation session. The risk of seizure initiation has been shown to be relatively low when applying 0.5 Hz pulses. Stimulation parameters were selected based on literature data (37, 46), and our previous experience that 0.5 Hz stimulation above 10 mA does not provide significantly better evoked responses, however it increases the risk of inducing seizures (10).

III.6. Analysis of SPES evoked potentials

Data analysis was performed using Neuroscan (Compumedics, El Paso, TX), EEGLAB (78), and custom MATLAB scripts (MathWorks, Natick, MA). Evoked responses to stimulation were divided in 1250 ms epochs (250 ms pre-stimulation to 1000 ms post-stimulation) time-locked to stimulation pulse delivery. Following low-pass filtering (20 Hz, 48 dB/oct) and baseline correction (− 250 to − 50 ms), the raw LFP signals were averaged in each grid pair stimulation trial. CCEP components' peak amplitude was measured as the absolute peak voltage between 5 and 500 ms. Z-score was computed using the standard deviation (SD) of baseline (− 250 to − 50 ms). Evoked potential latency was defined as the time from stimulus to peak of each component. The ratio of each detected component and the total recording on LME channels for each patient were determined, including all grid stimulation sites that triggered LME responses. The ratio of triggerability of individual components by layer and by distance from stimulated grid contacts, was also analysed (Fig. 2d). LFP, CSD, MUA, TFR, SUA analyses (Figs. 2c, 3, 4, 5, 6) and peak latency across channels (Fig. 2d/2) were examined in stimulation sites yielding the highest amplitude response (see Fig. 1e, yellow dots, for the location of preferred stimulation sites) on signals averaged across stimulation trials. In case of measuring peak latency pooled across channels and patients (Fig. 2d/1) and rate of evoked components (Fig. 2d/3–6) all stimulated sites with visible CCEP were included. When examining the layer-by-layer distribution of CCEP N2 and SW downstate, amplitude values (Figs. 4d and 6a–c and Fig. 16) of each patient were normalised across LME channels (10).

DOI:10.14753/SE.2025.3208

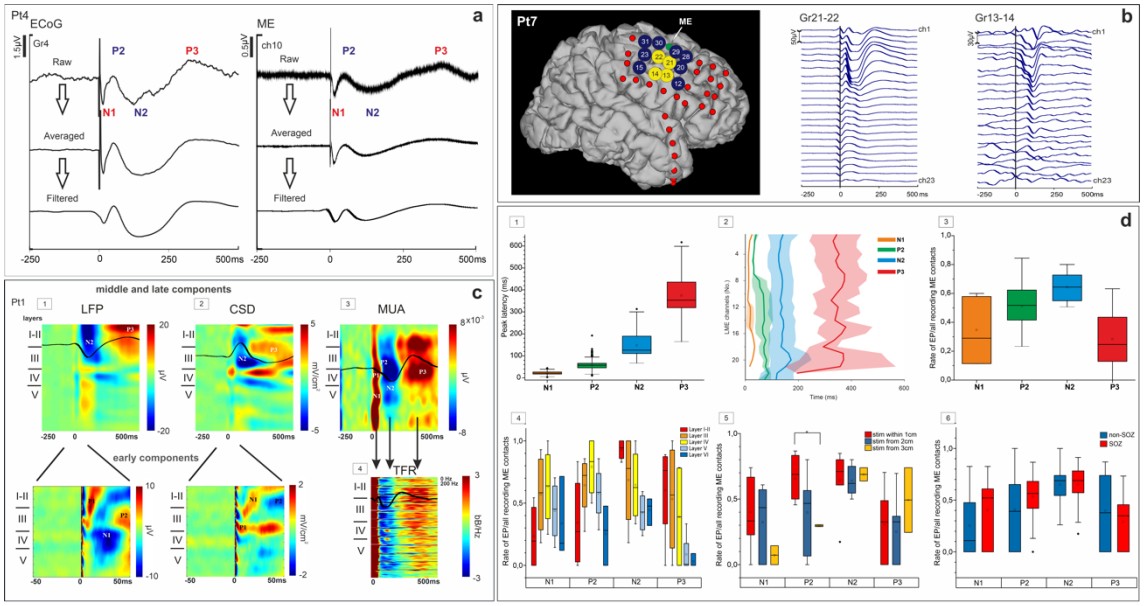

Figure 2. CCEP components (10). *(a)* CCEP components remain consistent across signal processing methods in both ECoG and LME recordings. *(b)* Single-trial example (Pt7) shows early components evoked from LME-adjacent ECoG contacts (Gr21-22) and middle/late components triggered from distant ECoG contacts (Gr13-14). *(c)* Laminar profile of CCEPs illustrated by the recordings of Pt1 (averaged across trials of a single stimulation site) shows LFP (c/1), CSD (c/2), MUA (c/3), and TFR (over 0-200Hz, c/4) aligned to stimulation. *(c/1) and (c/2) bottom row*: zoomed in to make early components more visible. Note that zoomed-in figures are unfiltered to make P1 component visible, while those in the top row are filtered with 20 Hz (48 dB). White and black curves mark the activity on the max-amplitude channel. The early components consist of a surface positivity with lower-middle layer sink (P1) and surface negativity with superficial sink (N1), accompanied by elevated MUA. The middle components consist of surface positivity (P2) with superficial source and surface negativity (N2) with wide middle layer source, accompanied by marked decrease in MUA. P3 is characterised by surface positivity with middle layer sink and upper-middle layer increase in MUA. The spectral power shows increase during early and late components and decrease during P2 and N2. *(d)* Peak latencies of LFP components (n = 7): pooled over all LME channels (mean, median, 1st and 3rd quartiles; **d/1**); across LME channels with no significant depth-dependent change (**d/2**). Considering the total number of detected components, N2 is evoked at the highest rate (n = 7, **d/3**). Although statistically non-significant, N1 and P2

components tend to be evoked in middle-, while N2 and P3 in supragranular layers (n = 4, **d/4**). The appearance of components is distance-dependent: N1 and P2 are most likely evoked within 1 cm from LME, P3 rather from a distance and N2 both up close and from further away (n = 7, **d/5**). There are no significant differences between stimulation from SOZ vs. non-SOZ, regarding appearance of components, though there is a tendency that N1 and P2 can be better evoked from SOZ (n = 7, **d/6**) (see "Results" for details of statistics).

III.7. Wide-band spectral power, current source density (CSD), multiple unit activity (MUA) and single unit activity (SUA) analysis of CCEPs and sleep spindles

In the CCEP study, following removal of stimulated channels and bad epochs (> 500 μV: − 250 to − 10 ms or 50–1000 ms), base- line correction (− 250 to − 50 ms) was applied. Time–frequency response (TFR) analysis for spontaneous and stimulation-induced oscillatory power changes between 1 and 200 Hz was computed and visualized on event-related spectral perturbation (ERSP in dB) maps (78) for each LME channel, in case of 2 patients (Pt1, Pt2), where the quality of the recordings was sufficient to obtain meaningful measures. Single-trial ERSPs were averaged and plotted on depth-versus-time color maps. Significant decrease and increase in ERSP was marked with color blue and red, respectively (see below for details regarding statistical analysis). CSD analysis (79) was done by second spatial derivation of LFP trial-averages after spatial hamming-window smoothing (detailed by Ulbert et al. (4)) and filtering (low pass, 20 Hz, zero phase shift, 24 dB/oct). In our case the raw LFP signal was inherently the first spatial derivative of the field potentials since it was recorded as gradual bipolar montage between contacts along the laminar electrode's shaft. We applied a second derivation to get the CSD signal: positive values are present where summed transmembrane currents exit the neighboring neurons (source), while negative values are measured where current enters the neurons (sink).

In the spindle study, to quantify laminar differences in field potential and current strength, the root mean square (RMS) of the LFPg and CSD signal of each channel was calculated for each 1 second LME data segment. Channel-wise RMSs were averaged across channels in the same cortical layer, yielding an average of LFPg and CSD signals for each spindle

and for each cortical layer (LFPg/CSD magnitude). One-dimensional averaged CSD data are presented on depth-versus-time maps, with color-coded sink (red) and source (blue) amplitudes. CSD was calculated for each patient (n = 4 in spindle, and n= 7 in CCEP study). MUA was calculated using high frequency filtering (1) 500–5000 Hz, zero phase shift, 48 dB/oct; (2) full wave rectification; (3) low pass filter: 20 Hz, 24 dB/oct) on individual sweeps. The sweeps, averaged across epochs, are visualized on depth-versus-time maps as color-coded activity increase (red) and decrease (blue) in population activity. MUA was triggered to ECoG spindle detections in a similar manner as LME data from the EEG range and averaged across detections by spindle type (slow/fast, local/global). The quality of the recording allowed MUA calculation for only 2 patients (Pt1, Pt2) in both spindle and CCEP studies. Single-unit activity (SUA) analysis was performed on LME data recorded with high sampling rate (20 kHz) in case of one patient (Pt1) in CCEP and two patients (Pt1, Pt2) in spindle analysis, where individual cell activities could be separated reliably from MUA/field activity and background noise. LFPg, CSD and MUA analysis was performed using Neuroscan (Compumedics, El Paso, TX), EEGLAB (78), and custom MATLAB scripts (MathWorks, Natick, MA). SUA was detected on epoched raw LME data sampled at 20 kHz (from − 250 to 1000 ms relative to stimulation start for CCEPs and ±1000 msec around all ECoG spindle peaks, separately for slow, fast, local, and global spindles). After DC offset removal, we detected SUA with an amplitude threshold adjusted manually according to the magnitude of background noise of each channel. Multiple individual neurons were identified as the generators of SUA on each channel based on clustering with on-line template setup by action potential morphology and amplitude in a 0.4 ms timeframe. We applied a principal component analysis based on template waveform correlations to refine clustering and reduce false detections. Then each cluster was revised visually. All SUA detections were performed in Spike2 (version 7 software (CED Limited, UK). All SUA detections were pooled from all cells on the same channel and from all LME channels in the same layer, resulting in time histograms of CCEP-associated single-unit firing (Fig. 3). Histograms of single trials were then averaged across stimulation epochs corresponding to one stimulated channel-pair. SUA occurrence relative to LFPg spindle phases was calculated based on the instantaneous phase angle of LFPg signal's Hilbert transform. All SUA detections within ±500 msec from ECoG spindles of the same spindle type were pooled from all cells on

DOI:10.14753/SE.2025.3208

the same channel and from all LME channels in the same layer, while the rest more temporally removed from ECoG spindle peaks were discarded (Fig.9) (9, 10).

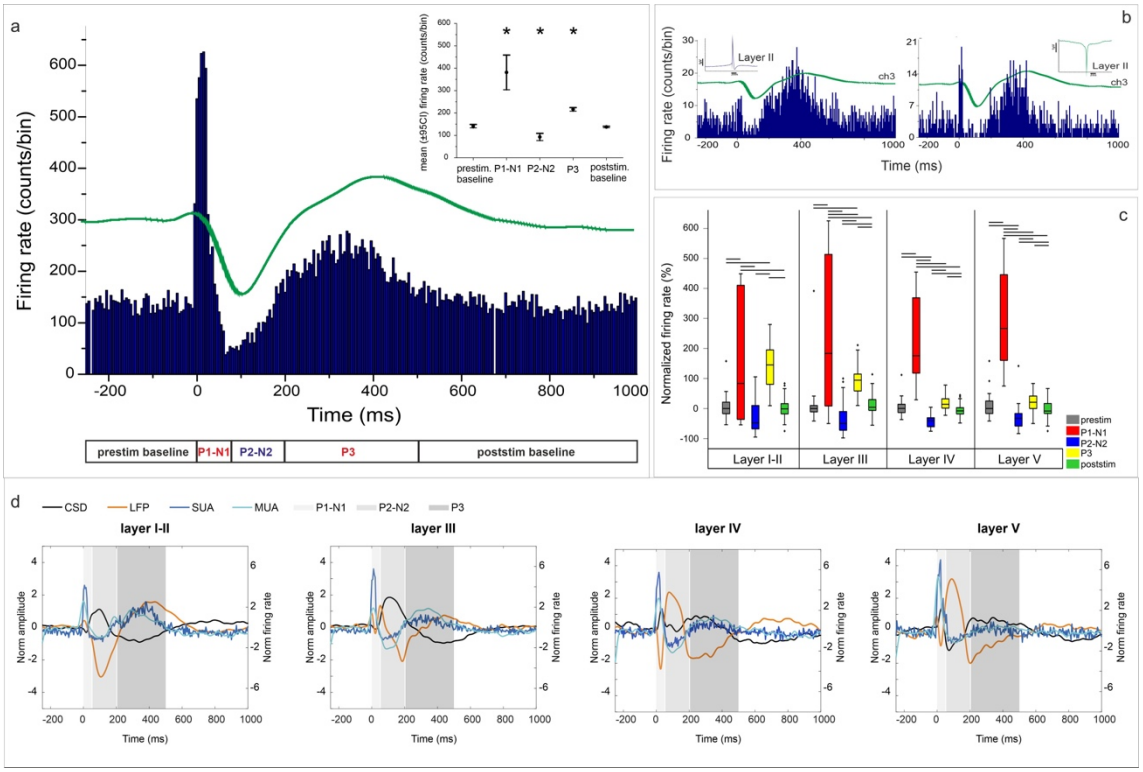

Figure 3. Single-unit correlates of CCEPs (10). *(a)* Average time histogram of neuron firing (n = 26, Pt1) shows sequential firing rate changes after stimulation. Increased firing occurs during P1-N1 (0–50 ms) and P3 (205–500 ms), while firing decreases during P2-N2 (55–200 ms). Asterisks on error bar plots indicate statistically significant differences in firing rate between all CCEP intervals and also between each interval and pre-and poststim. baseline periods (Kruskal–Wallis ANOVA; $\chi^2(4) = 151.8$, $p < 0.001$. Mann–Whitney U post- hoc tests, $p < 0.01$) *(b)* Firing rate changes in two neurons from layer II. *(c)* Largest firing change occurs in layer V during P1-N1; significant firing changes are noted in all layers (ANOVA with Bonferroni post-hoc tests, $p < 0.001$). Boxplots represent median with interquartile range (IQR), whiskers mark the most extreme values within 1.5xIQR. Crosses mark outliers outside this range. *(d)* LFP (orange), CSD (black; negative value=sink, positive value= source), MUA (light blue), and SUA (dark blue) overlays in Pt1, averaged per layer. Shaded areas represent the same time-windows as in case of (**a**)

DOI:10.14753/SE.2025.3208

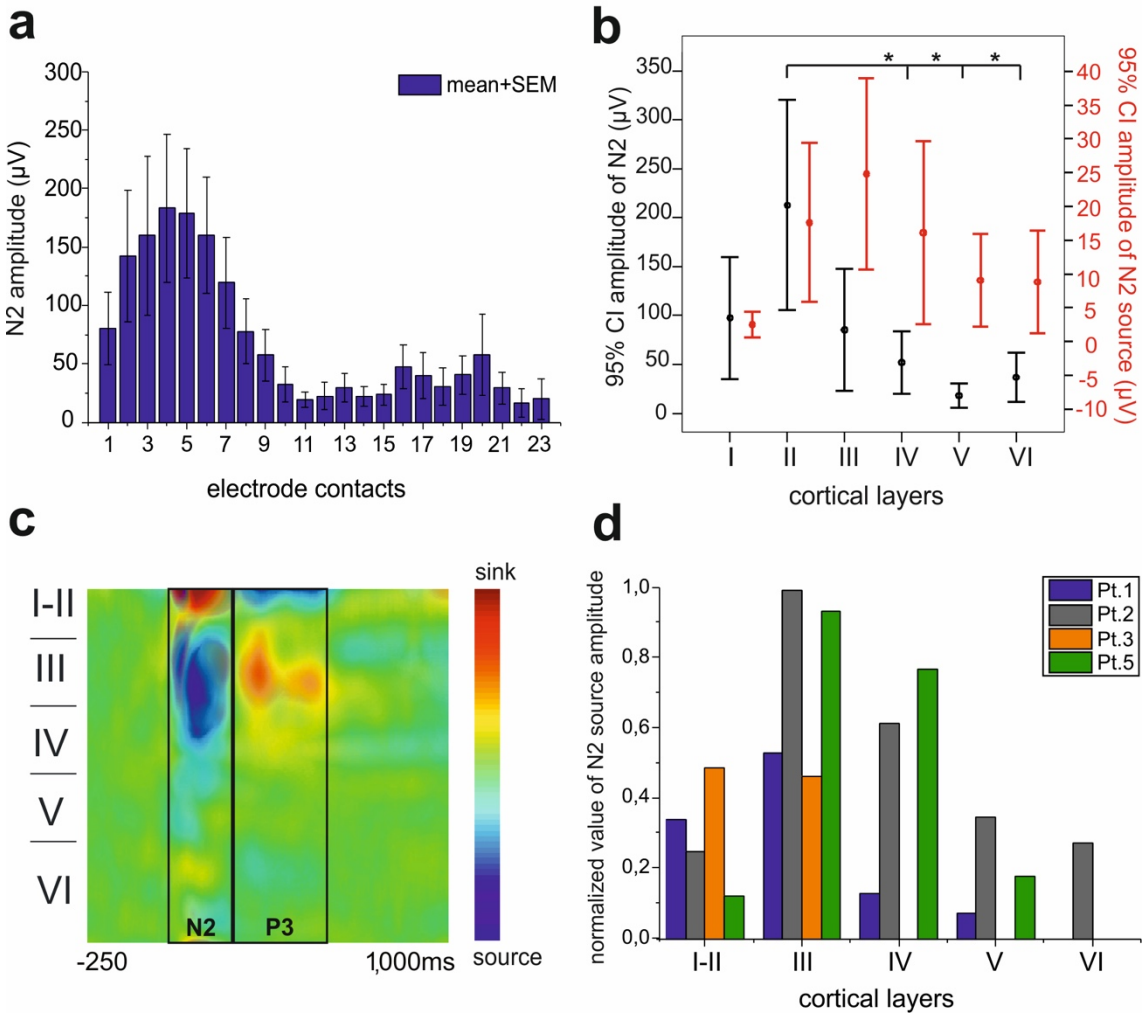

Figure 4. Laminar Distribution of N2 LFP, Current Sinks and Sources (10). *(a)* N2 field potential gradient changes across microelectrode contacts, averaged across trials, in 7 patients. *(b)* Significant N2 amplitude differences between cortical layers in 4 patients with histological data (one-way ANOVA ($F(5)=7.7$, $p<0.001$, $\eta^2=0.336$ and Tukey HSD post-hoc test $t_{II\text{-}IV}=4.3$, $p<0.001$, $t_{II\text{-}V}=5.77$, $p<0.001$, $t_{II\text{-}VI}=4.89$, $p<0.001$; black bars). No significant difference in N2 CSD source amplitude across layers (red bars). *(c)* Biphasic distribution of current sinks and sources in CCEPs across cortical layers, shown for 6 patients. *(d)* N2 current source peaks in middle layers, around layer III, normalized to each patient's peak response.

DOI:10.14753/SE.2025.3208

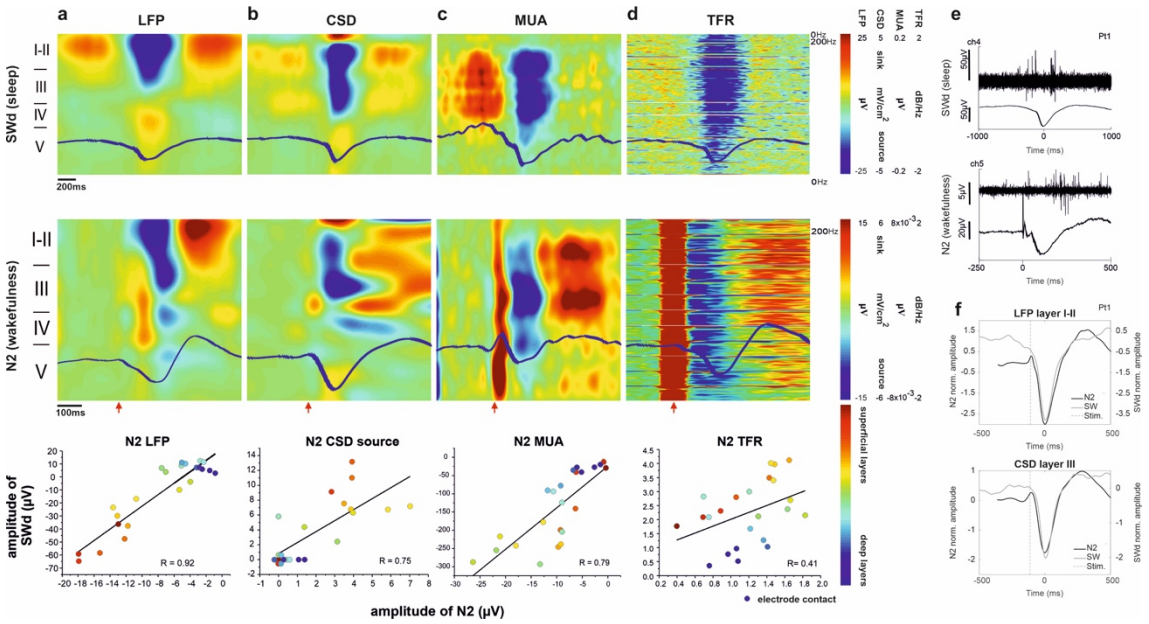

Figure 5. Electrically induced N2 during awake state is similar to the downstate of spontaneous slow waves (SWd) during sleep (10). *(a–d, Row 1)* Laminar profile of spontaneous SW time locked to downstate, showing upper layer negativity (LFP), middle layer source (CSD), decreased MUA, and broadband power decrease across layers (trial-average of Pt1). *(Row 2)* Laminar profile of CCEP in awake state (trial-average of Pt1): N2 shows superficial negativity (LFP), middle layer source (CSD), reduced MUA, and broadband spectral power decrease. Note the time scale differences between the two analyses (− 250–1000 ms for the N2 and − 1000–1000 ms for the SWd). Red arrows indicate the time of stimulus. *(Row 3)* Statistical comparison of SWd and N2 using Pearson's correlation (For LFP r = 0.92, CSD source r = 0.75, MUA r = 0.79, TFR r = 0.41, $p < 0.05$). The different color dots indicate individual electrode contacts. The warm color dots are for contacts located in superficial layers, the cold color dots indicate electrodes from deep layers. All data are derived from Pt1. *(e)* Averaged SWd and N2 waveforms (Pt1) on selected channels show neural silence. *(f)* Overlay of SWd (grey curves) and N2 (black curves) averaged waveforms in LFP and CSD. LFP (top) is derived from layer I-II, while the CSD (bottom) from layer III recordings (corresponding to the layers of maximal event amplitudes). Stimulation preceding N2 is marked with a dashed line.

III.8. Statistical analysis

Statistical analyses were performed using IBM SPSS (version 16.0), STATISTICA 10.0 (StatSoft, Tulsa, OK), JASP (version 0.18.3), jamovi (version 1.6.15.0) softwares and in-built Matlab (2018b, 2019b) algorithms. The statistical analysis of spindle SUA was performed using Oriana (v2.02c, Kovach Computing Services). Normality of distributions were tested with the Kolmogorov–Smirnov test. If normality was rejected non-parametric tests were applied, except for some cases (rate of appearance of CCEP components, Fig. 2d/3-4), when there were only moderate deviations from normality, acceptable in case of one-way ANOVA. To analyze the occurrence patterns of LME spindles and their co-occurrence with ECoG spindles, we used one-way ANOVA, the two-sample Kolmogorov-Smirnov test, Fisher's r-to-z transformation, and Pearson's correlation (Fig. 8, 9). For examining how spindle characteristics (including spindle type, globality, cortical layer, and amplitude measured by LFPg and CSD magnitudes) affected the laminar profile, we conducted mixed-effects ANOVA and principal component analysis (Fig. 11 and Fig. 12). To assess LFPg and SUA coupling, we applied Rayleigh's Z-test for circular uniformity. For examining the effects of layer and spindle type on the preferred phase of SUA-LFPg coupling, we used circular factorial ANOVA (Harrison-Kanji test) with Mardia's test for post-hoc comparisons (Fig. 13). To test the temporal consistency of CCEP components across cortical depth we calculated peak latencies of each component for each LME channel (7 patients) and used one-way ANOVA to test the significance of differences between LME channels (Fig. 2d/2). To compare the rate of evoked potentials across LME contacts (7 patients, Fig. 2d/3) and cortical layers (4 patients, Fig. 2d/4), we have applied one-way ANOVA for each CCEP component). Rates of CCEPs were also compared according to stimulation distance (within 1, 2 or 3 cm from CCEP presenting LME contact), using Kruskal–Wallis with post-hoc Tukey–Kramer tests (Fig. 2d/5), and to stimulation site [seizure onset zone (SOZ) vs. non-SOZ], using Mann–Whitney U test (Fig. 2d/6). The firing rate (FR) of cortical neurons (n = 26) of one patient (Pt1) was compared across various time intervals: pre- (− 250 to − 5 ms) and poststimulation (500 to 1000 ms) baseline periods and time intervals corresponding to different CCEP components. First, units from all LME channels were pooled and the changes of FR in time were compared by Kruskal–Wallis ANOVA and Mann–Whitney U post-hoc tests (Fig. 3a). Then additional statistical tests were performed for each

cortical layer separately, using one-way ANOVA with Bonferroni post-hoc tests (Fig. 3c). We have analyzed in more details the intracortical laminar profile of N2 components across patients. For this purpose, we averaged the absolute value of LFP amplitude at each LME channel for N2 (Fig. 4a) and LFP and current source amplitude at each cortical layer, in four patients (Pt1, 2, 3, 5), where histology was available allowing precise localization of microelectrode contacts to cortical layer (Fig. 4b, d). To test the statistical significance of differences in absolute amplitude values (both for LFP N2 and N2 current source) between cortical layers (and also between supragranular layers: layer I-III and granular-infragranular layers: layer IV-VI), we applied one- way ANOVA with Tukey HSD post-hoc test and Kruskal-Wallis ANOVA with Dwass-Steel-Critchlow-Fligner post-hoc analysis, following the correction of significance level according to the number of comparisons (significance level: $p < 0.05$, corrected significance level: $p < 0.0033$). Results are shown on whisker plot [dot = mean; whisker = 95% confidence interval; asterisk = statistically significant difference] (Fig. 4b). We have compared the characteristics of sSW and N2 components, using LFP and CSD data of four (Pt 1,2,3,5) and MUA and TFR data of two patients (Pt 1,2) (Fig. 5), Pearson's r correlation method was used to evaluate the relationship between SW and N2 measures with $p < 0.05$ significance level criterion, and we presented the results on scatter plots [dots = channels of LME] (Fig. 5 row 3 and Fig. 6a). The significance of difference in normalized amplitude values between N2 and SW downstate was determined by two-sample t-tests for each cortical layer (Fig. 6b) and confirmed by two-sided permutation t-test (Gardner-Altman estimation statistics plots) (Fig. 6c) (80). Due to low sample size, Bayesian statistics were also applied: Bayesian ANOVA for the layer-by-layer and distance-dependent comparison of components and Bayesian Mann Whitney U test for the comparison of appearance rates in SOZ vs non-SOZ areas. To define the strength of evidence for correlation between N2 and SW downstate amplitude values in each cortical layer we performed Bayesian Pearson correlation (9, 10).

DOI:10.14753/SE.2025.3208

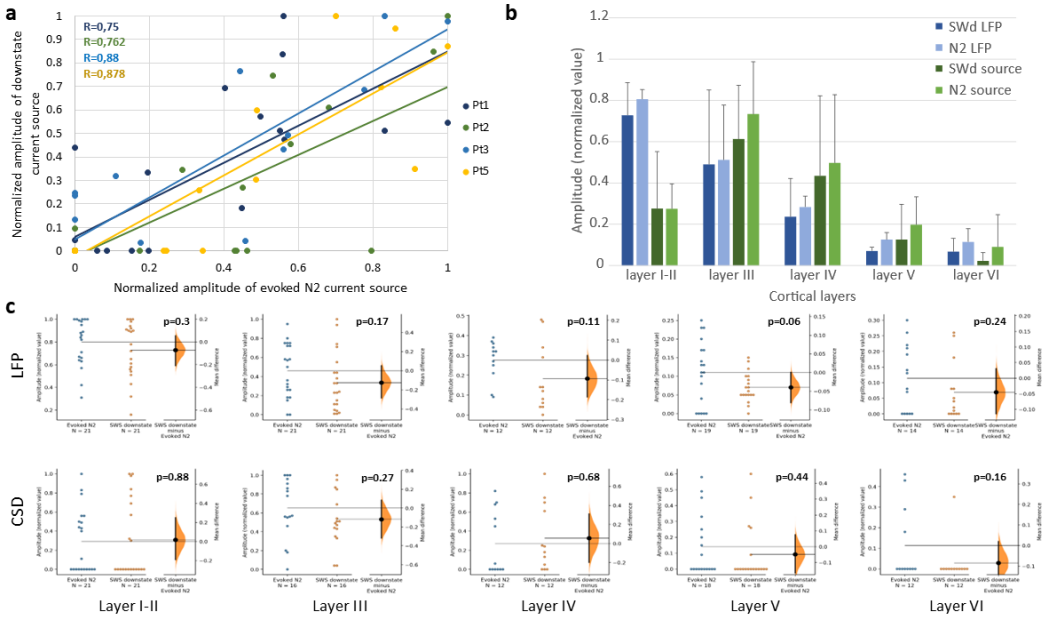

Figure 6. Similarities in the appearance of electrically evoked N2 and spontaneous SWd across cortical layers (10). *(a)* Scatter plots show a strong correlation in current source amplitudes for SWd and N2 in all four patients (Pearson's R for Pt1=0.75, Pt2=0.76, Pt3=0.88, Pt5=0.878). Color dots indicate electrode contacts; dots at 0 mark cases with undetectable N2/SWd. The dots in 0–0 locations represent more than one electrode contact per patient (for Pt 1 = 6, Pt2 = 9, Pt3 = 8, Pt5 = 11 contacts). *(b)* Averaged normalized field potential and current source amplitudes show no significant amplitude differences between N2 and SWd across cortical layers ($p > 0.05$, two-sample t-tests for each cortical layer). Maximal amplitudes occur in supragranular layers (field potential: layer I-II, current source: layer III). Data include four patients (Pt1,2,3,5) with histological reconstruction of electrode track; error bars indicate standard deviation. *(c)* Gardner-Altman estimation plots show non-significant mean differences in N2 and SWd amplitudes by cortical layer with 95% confidence intervals, indicating no statistical differences. Both groups are plotted on the left axes; the colored dots represent the individual electrode contacts; the mean difference is plotted on floating axes on the right as a bootstrap sampling distribution.

DOI:10.14753/SE.2025.3208

IV. Results

Clinical subdural grid and strip electrodes were implanted over the frontal, parietal and temporal cortices in seven patients to localise both the epileptogenic and eloquent cortical areas (Fig. 1e). Six patients had single focus (frontal n = 5; parietal n = 1; for detailed types of seizure onset see Table 1). One patient (Pt6) had multifocal seizure onset, therefore resective surgery was contraindicated in this case. LMEs (Fig. 1f) were implanted into the frontal lobe, underneath the subdural electrodes, in all seven cases (Fig. 1a,b). No clinical side effects or complications related to the multielectrodes were observed. Patients 2, 3, 4, 5 and 7 had a pathology of focal cortical dysplasia placed locally deep in sulci and gyri below the area marked by grey circles on Fig. 1e. Pt1 was MRI negative and Pt6 had a midline pathology (see Table 1). All the laminar electrodes fell outside the MRI lesion, but inside or very close to seizure onset zone (Fig. 1e). In four cases (Pt1, 2, 3, 5), histological reconstruction of the neocortical laminae was performed along the penetration track of the removed multielectrode (Fig. 1a–d). Electrode penetration tracks (Fig. 1a–d) showed intact cortical laminarization (well-preserved pyramidal cells, interneurons and glias, indicating no structural damage of the examined cortex). The thumbtack electrode successfully penetrated all six layers in three cases, while in one case (Pt1) the tip of the microelectrode ended in layer V. In the remaining cases (3/7), cortical areas sampled by LMEs were not removed according to the surgical plan (10).

IV.1. Characteristics of sleep spindles detected on surface and laminar electrodes

In the initial analysis, we identified spindle-like oscillations in LME recordings for 2 out of 4 patients (Patients 1 and 2), with visible oscillations and spectral peaks in the sigma range (8-16 Hz) matching those in ECoG data. For the other two patients, no visible LME oscillations or sigma peaks were detected. However, when LME recordings were aligned with ECoG spindle peaks, spindle-frequency oscillations emerged in the averaged LME signal, indicating sub-threshold spindle activity aligned with ECoG spindles (Fig. 7) (9).

DOI:10.14753/SE.2025.3208

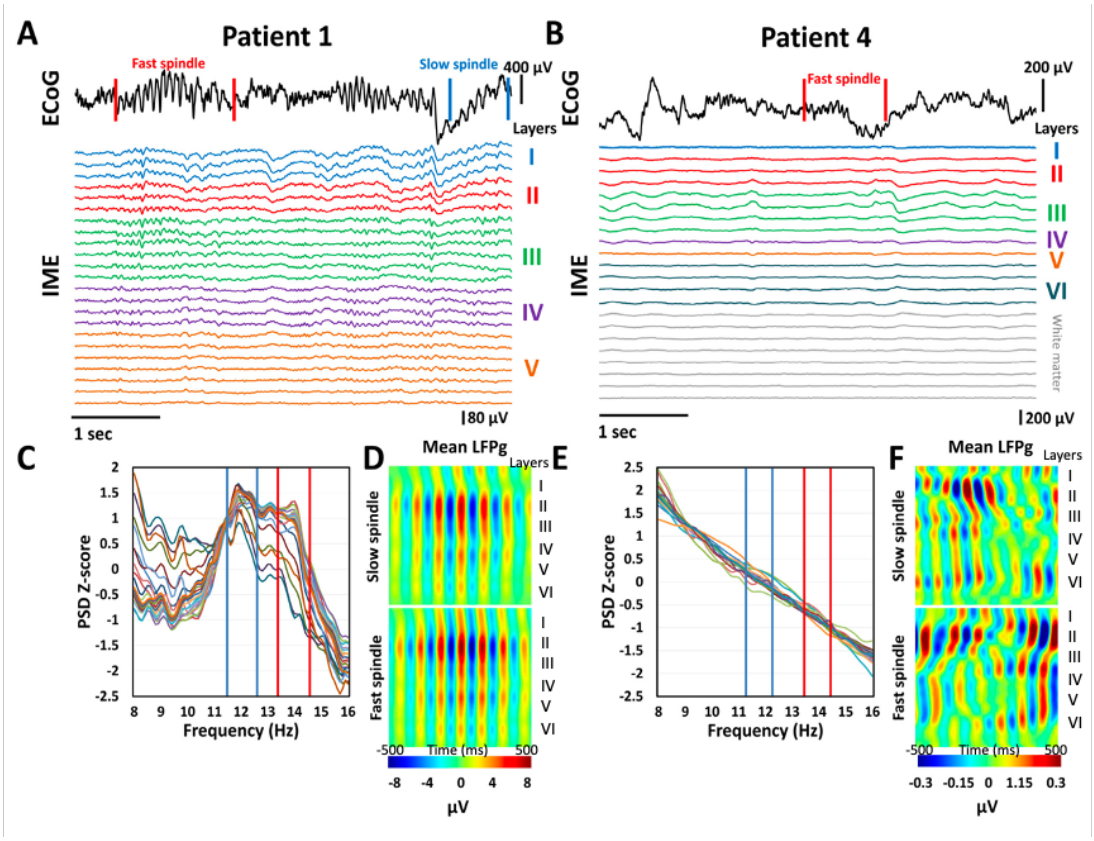

Figure 7. Sleep spindles are not always visible on LME LFPg recordings, but consistently appear when EcoG-triggered spindle detections are averaged (9). *(A)* In Patient 1, both slow and fast spindles visible on ECoG are also evident in LME recordings, with matching spectral peaks (Panel C shows z-transformed power spectral density; blue and red vertical lines indicate ECoG-derived slow and fast spindle frequency ranges, respectively. *(D)* Averaged LME LFPg triggered to ECoG spindle detections also reveals the presence of spindles on the LME during ECoG spindles. *(B)* In Patient 4, spindles are not visible in raw LME data nor create spectral peaks *(E)*, but averaging LME LFPg data triggered by ECoG spindle detections reveals spindles *(F)*.

Since spindle-like oscillations and sigma frequency peaks were observed in the LME signals of two patients at frequencies matching the ECoG signal, we further analyzed the occurrence patterns of LME spindles and their co-occurrence with ECoG spindles. We directly detected sleep spindles in the LME recordings of these two patients and compared them with ECoG spindle detections from the same recording sessions. While ECoG spindles showed slight location-based density variations (Fig. 8A), LME spindle density

was more uniform across layers (Fig. 8B), but had higher amplitude in superficial layers (Fig. 8C). In both ECoG and LME detections, most spindles were localized to a few channels or a single layer, with global spindles being rare (Fig. 8D-E). For both ECoG and LME, spindle amplitude increased with the number of channels or layers involved (Fig. 8 F-G). Density and amplitude measures are reported here as the mean density and amplitude, respectively, of all LME channels within a cortical layer. For the co-occurrence analysis, we considered two spindle events from sources s1 and s2 as co-occurring if the spindle in s2 began before the spindle in s1 ended, with s1 always marking the earlier event. For cortical layers, only spindles co-occurring in at least one-third of the channels within a layer were considered to account for the increased likelihood of simultaneous spindles with more channels. LME and ECoG spindles were considered co-occurring if they overlapped in any cortical layer and ECoG electrode. A significant proportion of spindles co-occurred across layers (50-80%) and between LME and ECoG (over 90% of ECoG spindles co-occurred with LME). Co-occurrence was more likely between neighboring layers, and LME-ECoG co-occurrence decreased with greater distance between electrodes. While LME-only spindles were common, most ECoG spindles had corresponding LME spindles (Fig. 9). We hypothesized that higher-amplitude LME spindles would be more likely to co-occur with ECoG spindles or appear on more ECoG electrodes. This was supported by a significant positive correlation between LME spindle amplitude and the spatial extent of co-occurring ECoG spindles in 13 of 20 cases, rather than the single case expected by chance (9).

IV.2. The laminar profile of sleep spindles

We found that micro-domain spindles detected on the LME show a heterogeneous cortical profile, consistent with previous findings (81). We then tested whether spindle type (slow/fast, local/global) influences spindle occurrence by cortical layer, as previously hypothesized (82, 83). No significant differences were observed in the density of slow vs. fast spindles across layers (X^2-test with row-wise z-tests, all $p>0.05$, Fig. 8/B). Additionally, we examined if ECoG spindle globality affected the layer of co-occurrence with LME spindles, finding no significant variation, except in Patient 2, where Layer V/VI spindles co-occurred with less global ECoG spindles (Fig. 10). Overall, the laminar distribution of LME spindles is heterogeneous, but similar across spindle types (9).

DOI:10.14753/SE.2025.3208

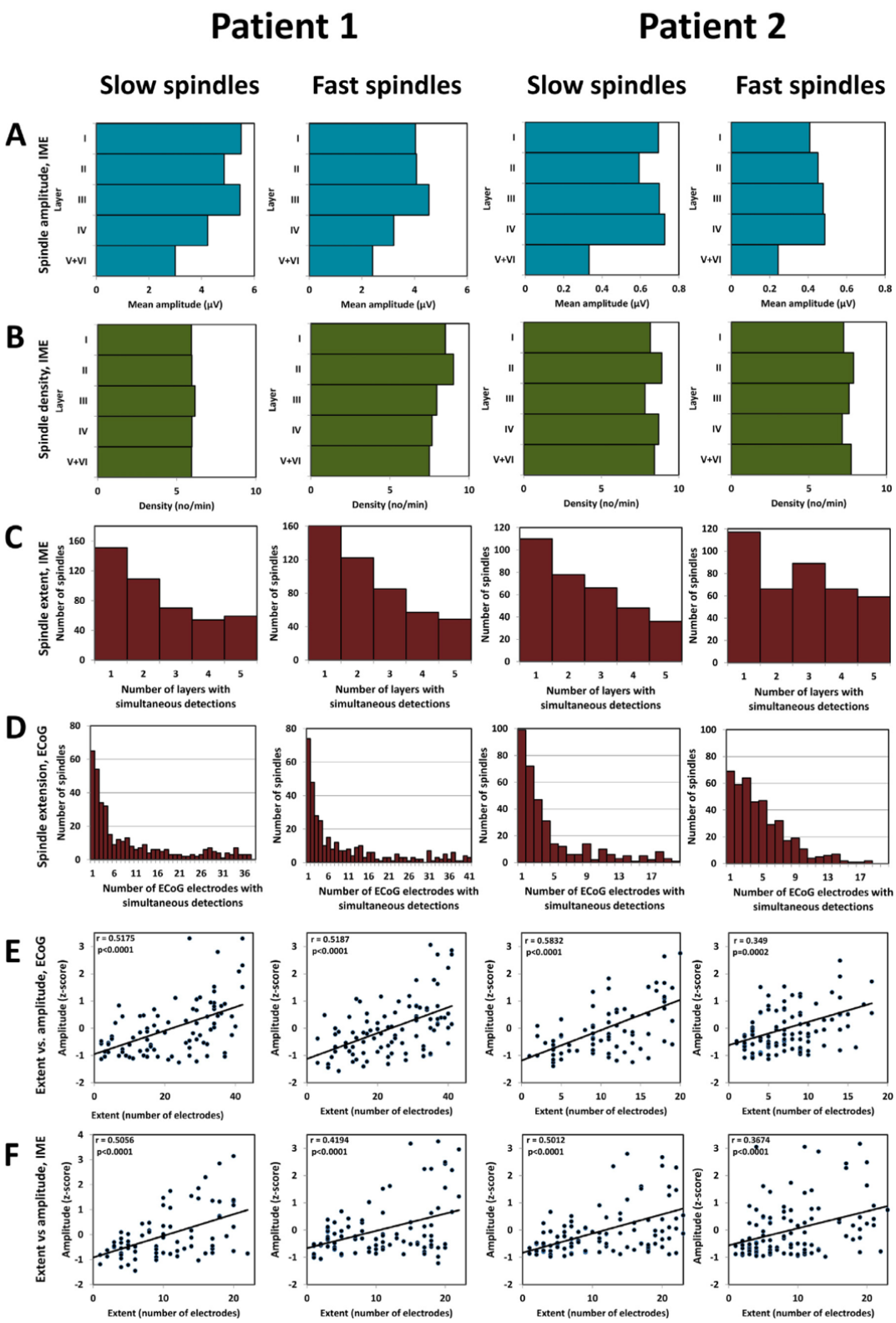

DOI:10.14753/SE.2025.3208

Figure 8. Sleep spindle characteristics on ECoG and LME (9). *(A, B)* Mean spindle amplitude and density by cortical layer on LME. *(C)* Histogram of spindle spatial extent on LME, showing the number of spindles detected across cortical layers (only spindles on at least 1/3 of same-layer channels were included; histograms show no significant difference, 2-sample Kolmogorov test, p_{min}=0.69 from all possible comparisons). *(D)* Histogram of spindle extent on ECoG, showing co-occurrences across channels (no significant differences; Kolmogorov test, p_{min}=0.27). *(E, F)* Correlations between spindle amplitude and extent on ECoG and LME, respectively. On ECoG spindle amplitude and spindle extent correlation coefficients are not significantly different (Fisher's r-to-z method, p_{min}=0.23 from all possible comparisons). On LME, slow spindles in Patient 2 show a stronger correlation with extent than fast spindles (p=0.044); other correlations are not significantly different (Fisher's r-to-z, p_{min}=0.13).

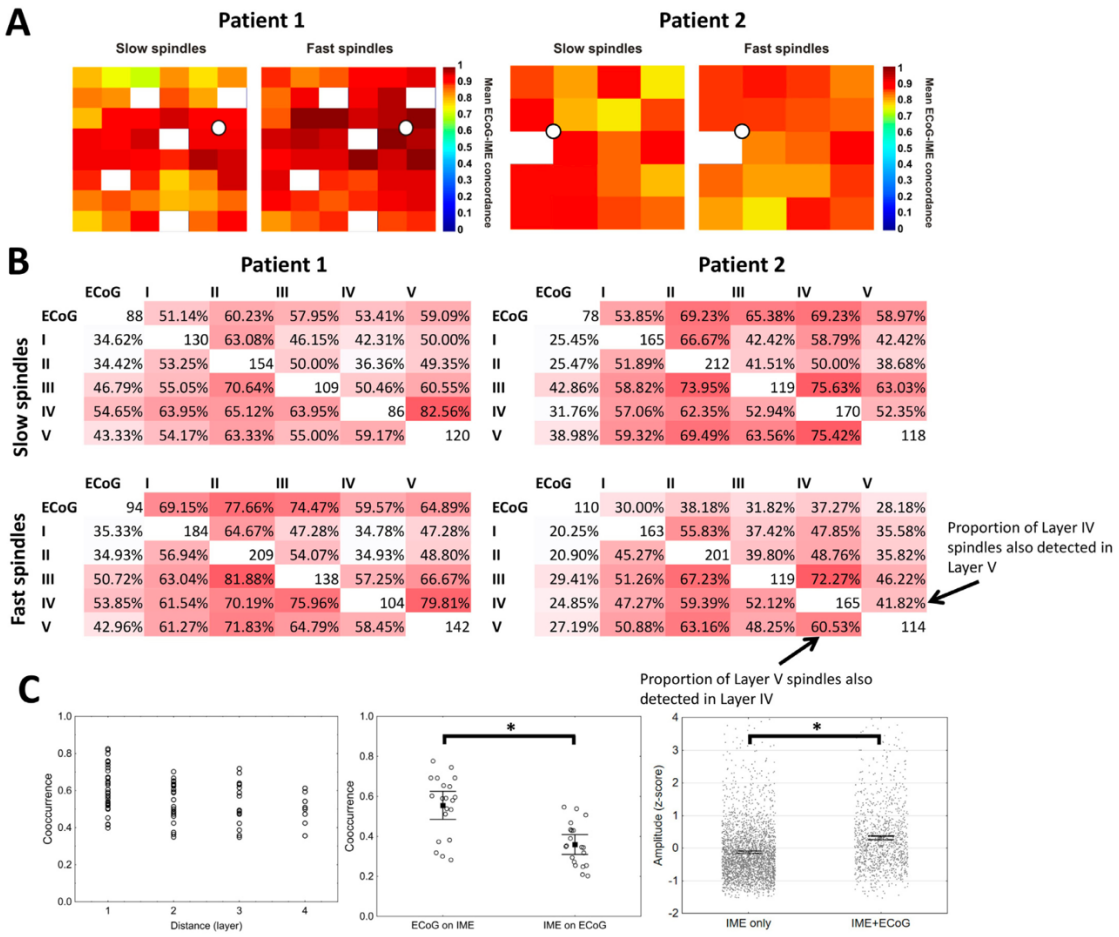

Figure 9. Co-occurrence of ECoG and LME spindles (9). *(A)* Proportion of ECoG spindles with a corresponding LME spindle in at least one cortical layer, shown on a

topographic map of the electrode grid (white dot = LME location). *(B)* Proportion and number of ECoG spindles co-occurring in specific cortical layers on LME and nearest ECoG channel for Patients 1 and 2 (only spindles on at least 1/3 of LME channels in the same layer included). The matrix shows layer-by-layer co-occurrence proportions. *(C)* Left: Co-occurrence probability decreases with layer distance (Pearson's r = -0.31, p=0.005). All spindle types from both patients were pooled for this analysis, within-patient and within-type correlations range between -0.28 and -0.37. Middle: ECoG spindles are more likely to co-occur on LME than LME spindles on ECoG (ANOVA F=22.65, p<0.001). The box and whiskers show means and 95% confidence intervals, individual data points (co-occurrence probabilities between ECoG and each layer from Panel B) are shown. Right: LME spindles co-occurring on ECoG have higher amplitude (F=166.6, p<0.001); pattern holds across layers (F=13.9–48.2, p<0.001).

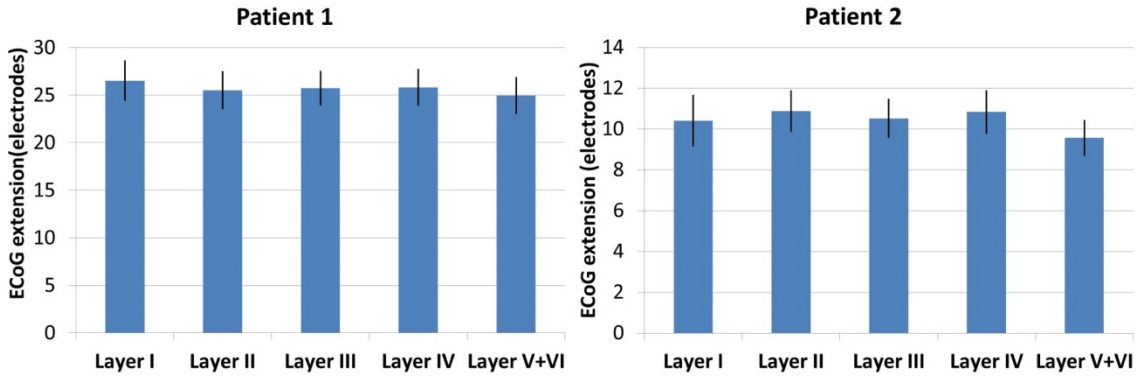

Figure 10. Spatial extent of sleep spindles (9). The extent (number of ECoG channels a spindle was detected on) of ECoG spindles co-occurring with LME spindles detected from each cortical layer in Patient 1 *(A)* and Patient 2 *(B)*. Error bars denote 95% confidence intervals. Slow and fast spindles were pooled for this analysis.

After confirming that sub-threshold spindle oscillations were present in all patients' LME recordings, we examined whether the laminar profile– that is, the characteristic pattern of LFPg and CSD amplitude across layers – of macro-domain (ECoG) spindles varied by spindle type (slow/fast) or globality (global/local). ECoG spindles, detectable over larger areas, were classified as macro-domain, while LME-detected spindles represented micro-domain activity. We detected sleep spindles in all physiological ECoG channels, and

DOI:10.14753/SE.2025.3208

triggered the signal of LME channels to the peaks of ECoG spindles detected from the ECoG electrode closest to the LME. Using a mixed-effects ANOVA, we analyzed how spindle characteristics influenced the laminar profile, with factors including spindle type, globality, cortical layer, and amplitude (LFPg and CSD magnitudes) as the outcome. We observed significant between-subject variability with intermediate effect size, and larger LFPg and CSD magnitudes were associated with more superficial layers, slow spindles, and global spindles. However, interactions of spindle type and globality with layer had small effect sizes (partial η^2_{max}=0.01), suggesting similar laminar profiles across spindle types within the same patient. These findings are illustrated in Figure 11 (9).

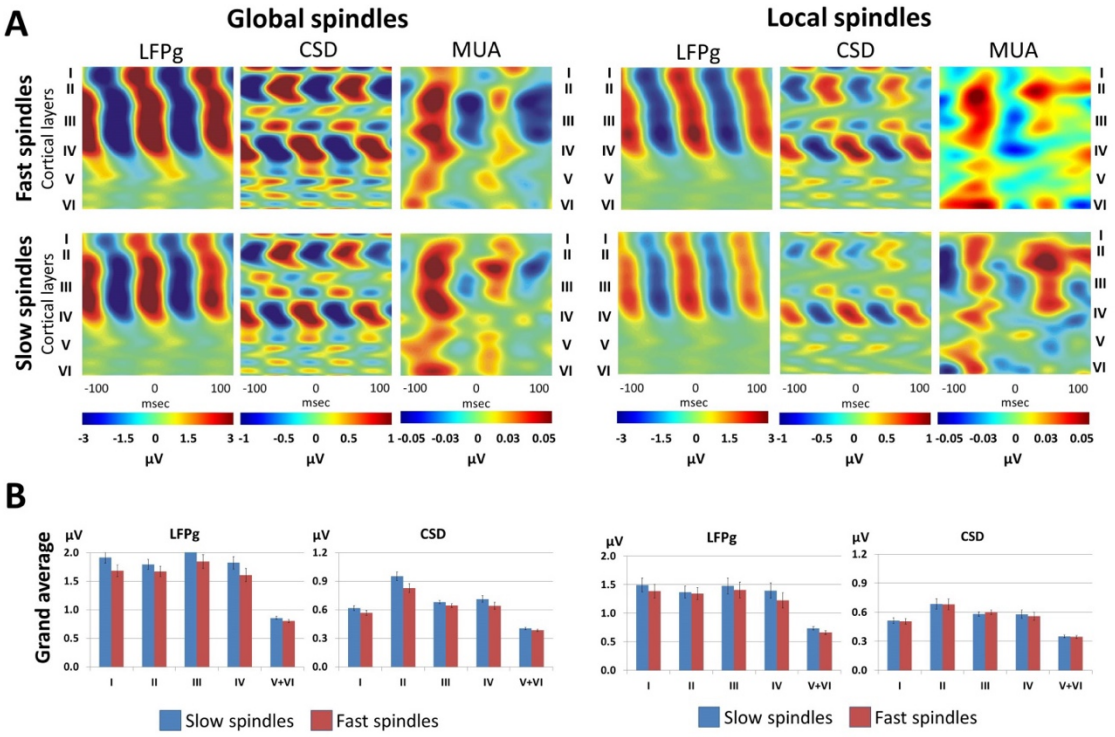

Figure 11. Laminar profile of sleep spindles (9). *(A)* The laminar profile of slow, fast, local and global spindles, including LFPg, CSD and MUA, in representative Patient 2. Color maps illustrate the average amplitude fluctuations ±100 msec before and after ECoG spindle peaks. Layer centroids are marked with Roman numerals. Note the similarity of the profile across all spindle types. *(B)* Grand average LFPg and CSD magnitude across layers for slow and fast spindles from all patients. µV values refer to µV/150 µm in case of LFPg and µV/150 µm^2 in case of CSD

DOI:10.14753/SE.2025.3208

To account for potential biases from individual differences in mean voltage, we repeated the analyses using z-transformed LFPg and CSD magnitudes across layers. This method removes between-subject main effects but retains sensitivity to interactions, allowing us to examine how spindle type and globality affect the laminar profile. Results were similar to the non-normalized model, showing substantial between-subject variability but similar laminar profiles for all spindle types within each subject (interaction partial η^2 max = 0.007). Further analyses using PCA confirmed that different spindle types (slow/fast, local/global) exhibit a consistent laminar amplitude pattern, suggesting similar cortical network involvement across types. Detailed results are shown in Figure 12.

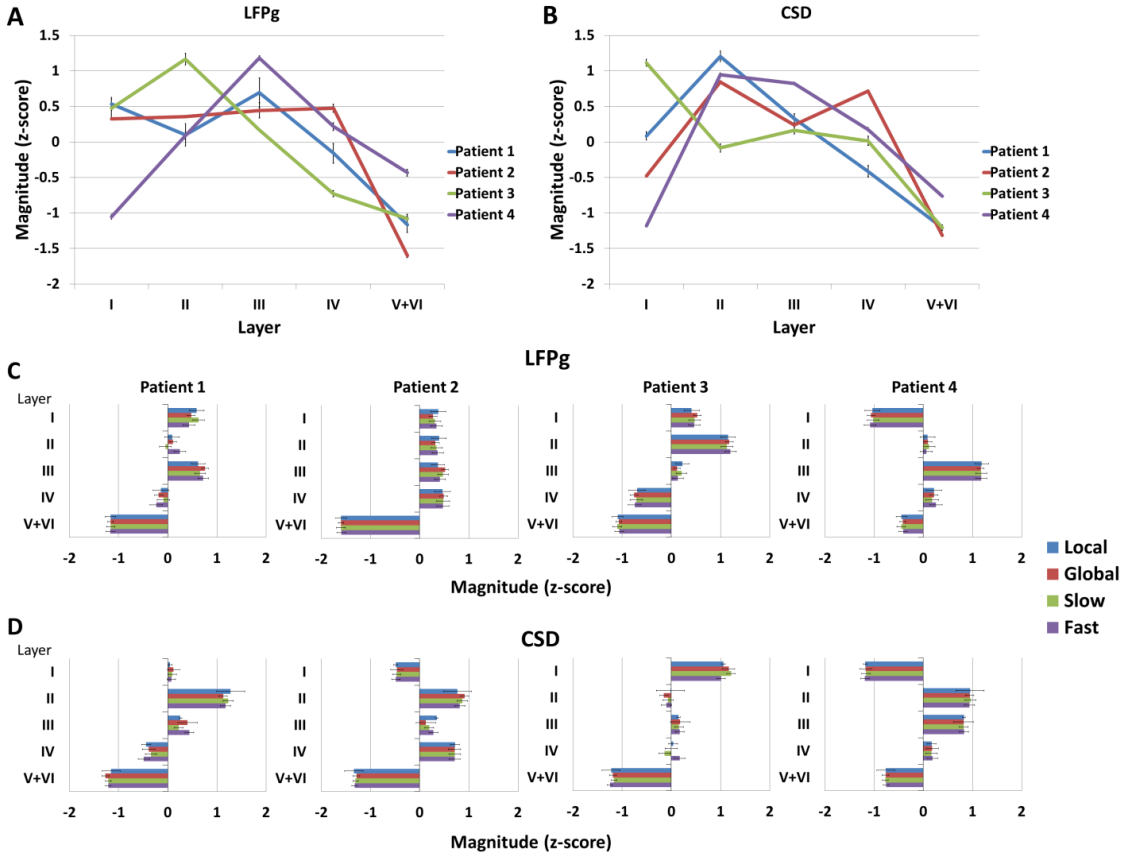

Figure 12. Normalized LFPg and CSD laminar profiles of sleep spindles (9). *(A, B)* Mean LFPg and CSD magnitudes by cortical layer for each subject. *(C, D)* LFPg and CSD magnitudes by layer and spindle type (local, global, slow, fast) for each subject. Error bars show 95% confidence intervals. Laminar profiles are similar across spindle types.

DOI:10.14753/SE.2025.3208

IV.3. Single- and multiunit correlates of sleep spindles

High-quality single-unit (SUA) and multiunit activity (MUA) was recorded from two patients (Patient 1 and 2, Table 1. spindle study). Based on a statistically significant deviation from circular uniformity, in Patient 1 SUA was significantly coupled to LFPg during all spindle types and in all layers except slow local, fast local and slow global spindles in Layer II and during fast local spindles in Layer V. In Patient 2, coupling occurred for slow and fast global spindles in Layers II and III. Slow local spindles in Layer II and fast global spindles in Layer VI were also significantly coupled. SUA preferentially occurred during positive-negative LFPg transitions when coupling was significant, in all patients (Fig. 13) (9).

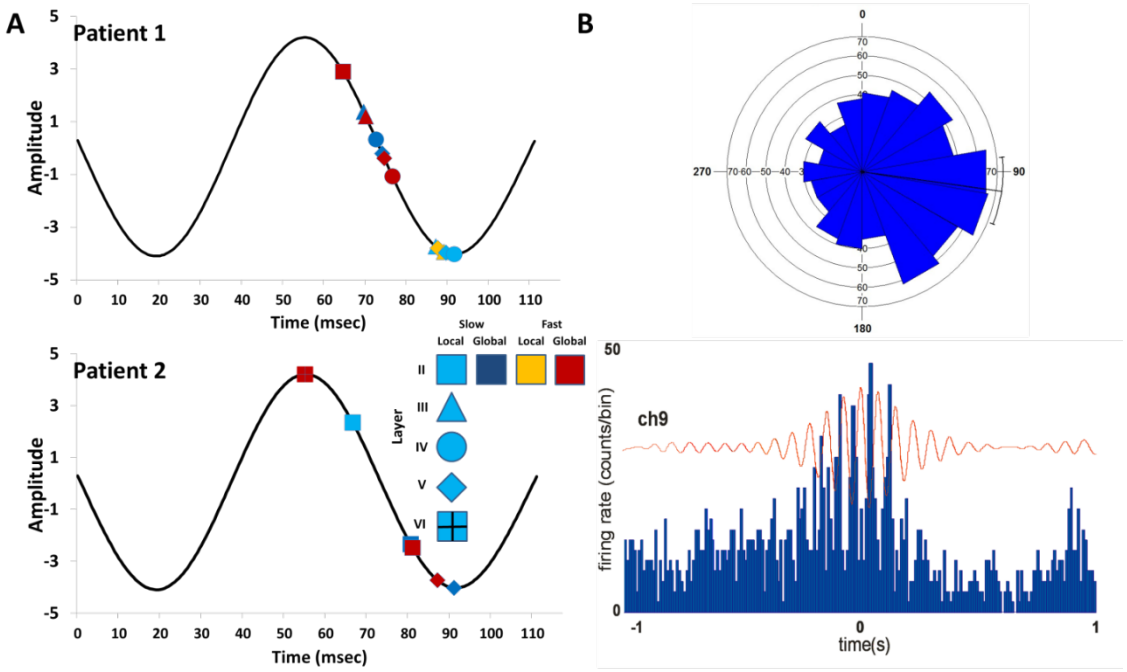

Figure 13. Preferred phases of SUA during spindles (9). *(A)* Preferred SUA phases during significant (based on Rayleigh's Z-test) LFPg-SUA coupling for each spindle type (coded by color) and cortical layer (coded by shape), overlaid on a typical spindle-frequency oscillation. *(B)* Example of SUA occurrence at positive-negative LFPg phase transitions during fast global spindles on a layer III channel in Patient 1. Rose plot shows preferred firing phase just after 90°, aligning with the first data marker in (A). Line histogram shows SUA frequency aligned with mean spindle LFPg on the same channel.

DOI:10.14753/SE.2025.3208

A circular factorial ANOVA (Harrison-Kanji test) showed a significant effect of both layer and spindle type on the preferred phase of SUA-LFPg coupling in both patients ($p < 0.001$). Post-hoc comparisons (using Mardia's test) revealed that in Patient 1, slow and fast spindles in the same layer had similar phase preference, which were however different for the same spindle types in different layers, and for local and global spindles even in the same layer. In Patient 2, similar trends were observed but reached significance only when comparing superficial and layer V-VI global spindles. MUA and LFPg signals, triggered to ECoG spindles, were generally correlated and showed an antiphase ($90° < \Delta\Phi < 270°$) relationship, as it was estimated by the angular mean of the difference of the phase angle of their Hilbert transforms (Fig. 14). However, the phase angle difference varied, particularly in Patient 2, reducing correlation consistency. Overall, SUA and MUA were negatively correlated to LFP, with variations by patient, layer, and spindle type (9).

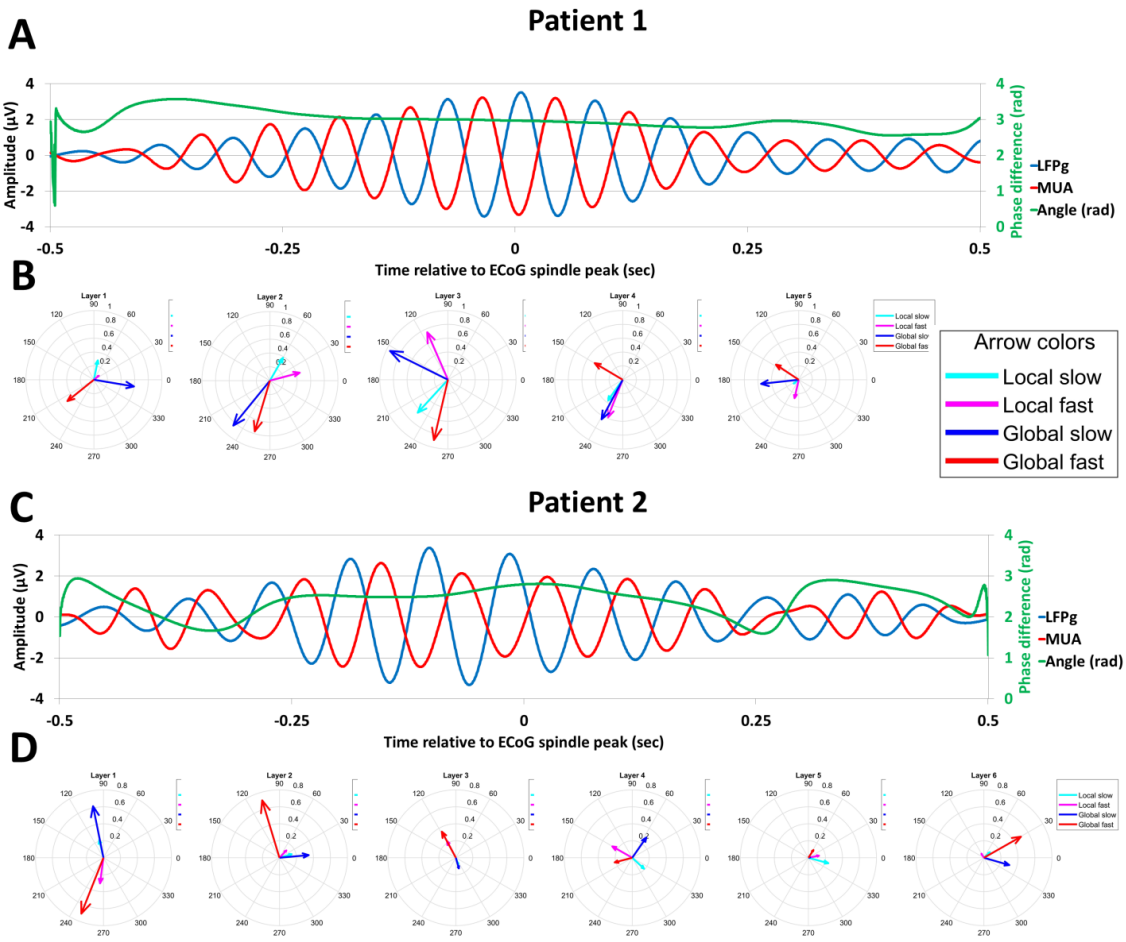

Figure 14. LFPg and MUA averages triggered to ECoG spindle events (9). *(A, C)*

LFPg and MUA averages from channel 10 (Layer III) in Patient 1 and channel 6 (Layer II) in Patient 2, showing fluctuations in phase differences. *(B, D)* Similarity of LFPg and MUA signals and their phase differences by layer and spindle type for each patient. In compass plots, arrow length represents the LFPg-MUA correlation coefficient, and orientation shows the mean phase difference.

IV.4. Characteristics and laminar distribution of CCEP components

CCEPs were recorded both with surface and laminar electrodes in seven patients (Fig. 1e). Characteristic components of CCEPs were identified and analysed: early (P1, N1), middle (P2, N2) and late (P3) evoked responses (Fig. 2a, Fig. 15), with special emphasis on N2. The appearance of P1 was less consistent compared to other components (it was found in only 3/7 patients) and was highly dependent on stimulation distance, mostly visible on adjacent surface electrodes (Fig. 2b, Fig. 15). Components of CCEPs could be clearly identified and were consistent, regardless of different signal processing methods (i.e. averaging and low pass filtering), both on ECoG and LME recordings, except for P1 which tended to smear with low-pass filtering (Fig. 2a, due to its inconsistent appearance of P1, it is not shown in this figure). The appearance of some components is distance-dependent, i.e. the early ones (P1, N1) can be triggered mostly from the vicinity of LME, while the middle and late ones (P2, N2, P3) can also be triggered from a more distant site (Fig. 2b and d/5). We have analysed the components using LFP and CSD data of seven, and using MUA and TFR data of two patients, in a time-window of − 250 to + 500 ms relative to stimulation. The resulting activation patterns were qualitatively very similar in all patients (Figs. 2c, 4c, 5 row 2, Fig. 15) and revealed different intracortical mechanisms in the background of CCEP components. Figure 2c shows the typical LFP, CSD, MUA and TFR patterns. LFP under P1 exhibits a maximal positivity and a sink-source pair located around cortical layer III, while there is a considerable sink also in deeper layers. It is associated with increased MUA and TFR, encompassing all cortical layers. The N1 component appears as a negative wave in layer III LFP and is linked to a sink in cortical layers I-II, and source pattern reaching to deeper layers, with increased MUA and TFR, mainly in infragranular layers (10).

DOI:10.14753/SE.2025.3208

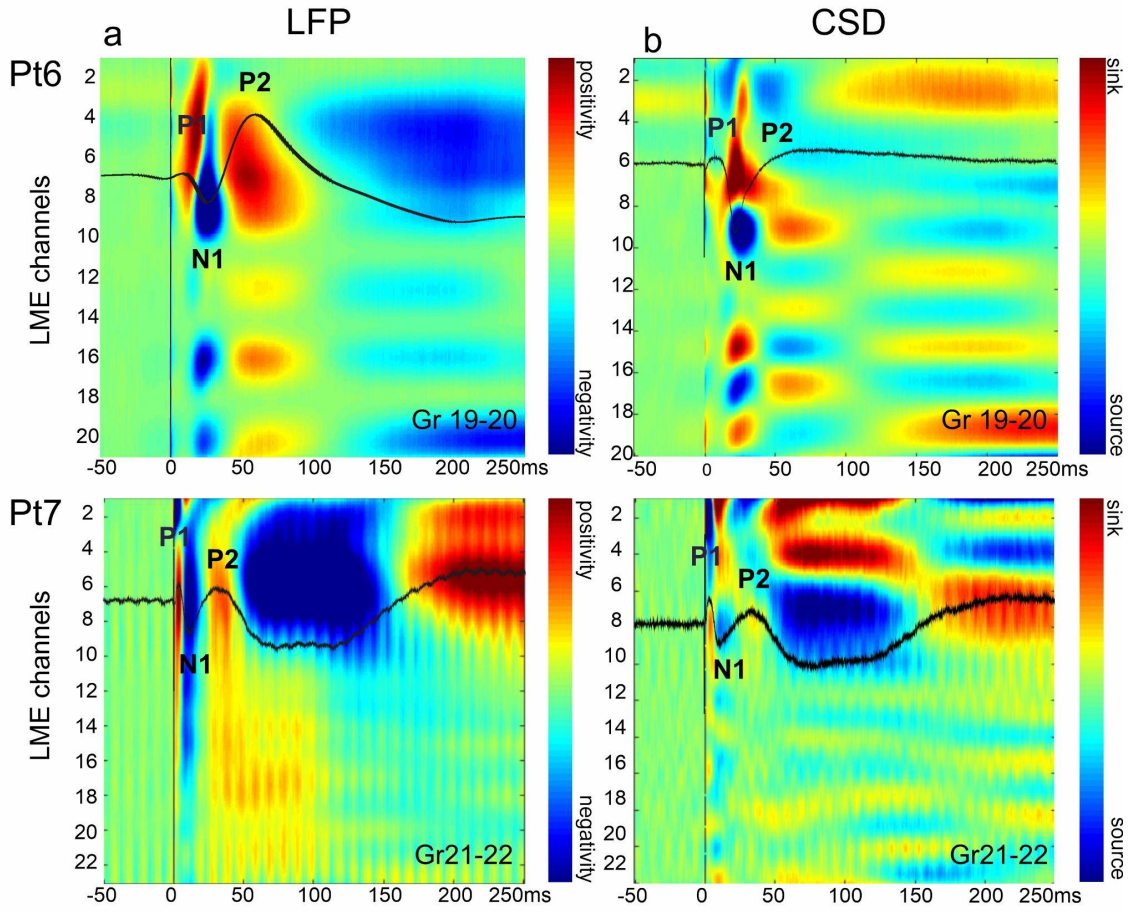

Figure 15. LFP and CSD patterns for early CCEP components (10). *(a)* LFP patterns for early CCEP components (P1, N1, P2) in 2 patients. *(b)* Corresponding CSD maps, noting that Pt6's map shows artifacts due to low recording quality, as CSD is sensitive to low signal-to-noise ratios.

The prominent positive wave seen during P2 in the LFP engages multiple layers and is associated with a source in cortical layers I–II, and decreased MUA and TFR power. The N2 shows the most marked negative deflection in layers I–III, while it is accompanied by a source in cortical layers III–IV with decreased MUA and TFR power during the descending phase across all layers (see more detailed description of N2 in next section). This LFP pattern is subsequently inverted (positive deflection) in upper layers during P3 component, which corresponds to a sink at layers III-IV concomitant with increased MUA and TFR in layers I–IV. MUA and TFR increase already starts at the ascending phase of

N2. It has to be noted that LFP, CSD, TFR and MUA were only analysed in preferred stimulation sites, i.e. those yielding the highest amplitude response. Nevertheless, the pattern obtained in non-preferred stimulation sites was similar to that presented above, although with lower signal-to-noise ratio (Examples for CSD patterns corresponding to preferred and non-preferred sites are presented in our scientific paper- (10)/ Suppl. Fig. S3). The peak latency of evoked components was measured on individual LME contacts. Latencies derived from all stimulation epochs with elicited responses and averaged across LME contacts and patients were, as follows (mean ± SD): N1 21.95 ± 7.16 ms, P2 57.47 ± 20.7 ms, N2 147.31 ± 51.7 ms, P3 374.88 ± 83.22 ms (Fig. 2d/1, n = 7). No significant difference was observed in latencies across cortical depth, as shown by the results of one-way ANOVA: N1 $F(20)=0.32$ and $p=0.96$; P2 $F(22)=1.3$ and $p=0.24$; N2 $F(22)=0.36$ and $p=1$; P3 $F(21)=0.33$ and $p = 1$ (Fig. 2d/2, n = 7). In this case only the epoch with the best response was used for each patient. The rate of appearance of each component was calculated considering all the CCEP-eliciting stimulations of all patients (mean ± SD): N1 0.35 ± 0.2; N2 0.64 ± 0.1; P2 0.51 ± 0.2; P3 0.28 ± 0.2. The highest rate was observed in case of N2 (Fig. 2d/3, n=7), which was significantly greater than the rate of N1 and P3 (one-way ANOVA $p = 0.0008$, $F (3) = 7.48$; post-hoc Tukey–Kramer). When dividing occurrence rates to cortical layers (n = 4, with histological reconstruction), N1 and P2 components appeared to be more frequent in middle (III-IV), while N2 and P3 in superficial (I-II-III) layers (Fig. 2d/4, n = 4), although these observations were statistically not significant (one-way ANOVA N1: $p = 0.388$, $F (4) = 1.116$, P2: $p = 0.124$, $F(4) = 2.183$; N2: $p = 0.081$, $F(4) = 2.606$; P3: $p = 0.182$, $F(4) = 1.813$). In both cases, normal distributions were tested with Kolmogorov–Smirnov test. Bayesian ANOVA showed only with anecdotal evidence that the rate of appearance of N1 and P3 components is not different across layers, and also with anecdotal evidence that the rate of appearance of P2 and N2 might be different across layers (for detailed statistical results (10)/ Supplementary Table S4). CCEPs elicited from varying stimulation distance contained different components at varying degree. N1 and P2 components were triggered most likely from within 1 cm, P3 emerged most often within 3 cm distance, while N2 seemed to be independent from stimulation distance (Fig. 2d/5, n = 7). These observations were confirmed by statistical testing only in the case of P2 evoked from 1 vs 3 cm (Kruskall–Wallis test, post-hoc Tukey–Kramer N1: $p = 0.1457$, $\chi^2(2) = 3.85$; P2: $p = 0.01947$, $\chi^2(2)$

= 7.88; N2: p = 0.68, $\chi^2(2) = 0.77$; P3: p = 0.4185, $\chi^2(2) = 0.41$) The result of Bayesian ANOVA show only anecdotal evidence also in this case: in favour of no distance-dependence in case of N1, N2 and P3 and in favour of distance-dependence in case of P2 (see our scientific paper (10)/ Supplementary Table S4). Normality of distributions was rejected in most cases, tested by Kolmogorov–Smirnov test. Figure 2b illustrates this by an example where early components are visible only following stimulation of adjacent electrodes, while later components emerged by the stimulation of more distant contacts. Whether a certain component can be triggered more often when stimulated from the SOZ, compared to non- SOZ areas, has not been confirmed by our analysis (Fig. 2d/6, n = 7). Although N1 and P2 components seem to emerge at a higher rate in case of SOZ stimulation, the difference was statistically not significant (Mann–Whitney U-test N1: p=0.3681, U=268.5; P2: p=0.80444, U=149; N2: p=0.90358, U=570; P3: p=0.05152, U=206.5 while the evidence provided by Bayesian Mann–Whitney U test was only anecdotal (for detailed statistical results see our scientific paper (10)/ Supplementary Table S4). Normal distribution was rejected by Kolmogorov–Smirnov test (10).

IV.5. Single unit correlates of CCEP

Analysis of SUA was performed in the case of one patient, with the highest quality recording (Pt1), resulting in 26 clustered cells. The firing pattern of detected neurons was examined during the time-windows of different CCEP components. Significant changes relative to pre- (from − 250 to − 5 ms) and poststimulation (500–1000 ms) periods were found (Kruskal–Wallis ANOVA; $\chi^2(4) = 151.8$, p = 0.0001, Mann–Whitney U post-hoc tests, $p < 0.01$). During P1 and N1 (0–50 ms), the firing rate of neurons increased significantly, followed by a significant decrease occurring in the time-window of P2 and N2 (55–200 ms). P3 window (205–500 ms) was again associated with increased firing activity (Fig. 3a, b). The same pattern was shown to be significant in all cortical layers (one-way ANOVA with Bonferroni post- hoc tests; layerI–II: F (4) = 67.47, $p = 2*10^{-38}$; layerIII: F(4) = 51.42, $p = 3*10^{-39}$; layerIV: F(4) = 129.21, $p = 4*10^{-54}$; layerV: F(4) = 115.17, p4*10^{-55}), although the changes relative to prestimulation window were most prominent in case of layer V (Fig. 3c). Temporal association of spiking activity, MUA, CSD and LFP has been visualised by overlaying these time series (Fig. 3d) (10).

IV.6. Laminar distribution of CCEP N2 component

Intracortical amplitude distribution of N2 is shown in Figs. 4a,b, 5a row2, 6b and Fig. 16. LFP under N2 of 7 patients showed negative deflection with amplitude maxima in the upper channels (Fig. 4a, n = 7). N2 amplitude of the 4 patients with histological reconstruction was significantly greater in supragranular (I-III) versus infragranular (IV-VI) layers (0.7 versus 0.15, grand average for baseline normalised values, Mann–Whitney U-test (U = 452, p = 0.0001). The greatest amplitude was observed in layer II (Bonferroni adjusted at $\alpha = 0.0033$). Layer II showed higher amplitudes than layer IV ($t(5) = 4.3$, $p = 0.001$), layer V ($t(5) = 5.77$, $p = 0.001$) and layer VI ($t(5) = 4.89$, $p = 0.001$) (one-way ANOVA and Tukey HSD post-hoc test with Bonferroni correction ($F(5) = 7.7$, $p < 0.001$); Fig. 4b black bars, n = 4). Regarding the CSD analysis, there was a prominent source under N2, qualitatively very similar in all patients (Fig. 4c overlaid maps of n = 6 patients). The detailed quantitative analysis of N2 reflected that the source was present in all layers but primarily involving the middle-upper layers with a maximum in layer III (Figs. 4b, d and 6b, n = 4). We observed greater amplitudes in supragranular versus infragranular layers (0.45 versus 0.25, grand average for normalised values, n = 4, Mann–Whitney U-test, U = 599, p = 0.031). Layer-by-layer comparison resulted in slightly significant differences revealed by Kruskal–Wallis ANOVA ($\chi^2 = 16.7$, $p = 0.005$), although post-hoc tests did not show any relevant differences between layers (Fig. 4b red bars, 4d, n = 4) (10).

IV.7. Comparison of spontaneous slow wave (sSW) and CCEP N2 component

We defined the laminar characteristics of sSW in four cases where histological reconstruction of microelectrode track was available (Pt1, 2, 3, 5), in order to compare the two types of negative potentials (i.e. the N2 and downstate of sSW) quantitatively. The total nr. of identified SWs for each patient and examples for raw recordings of sSW and N2 are shown in our scientific paper (10)/ Supplementary Fig. S3 and Suppl. Table S3. Figure 5 illustrates the data of one patient (Pt1), while the results of the other three subjects can be found on Fig. 6, 16 and (10)/ Supplementary Fig. S4. Similar to our previous findings, the SWd was characterised by a negativity maximal in supragranular layers (I-III, Fig. 5 row1/a, (10)/Supplementary Fig. S4), a current source highest in the

DOI:10.14753/SE.2025.3208

middle-upper layers (II-IV, Fig. 5 row1/b) and a MUA decrease in the middle layers (II-IV, Fig. 6 row1/c), accompanied by a pronounced wideband (1–200 Hz) spectral power decrease across all cortical layers (Fig. 5 row1/d) (10).

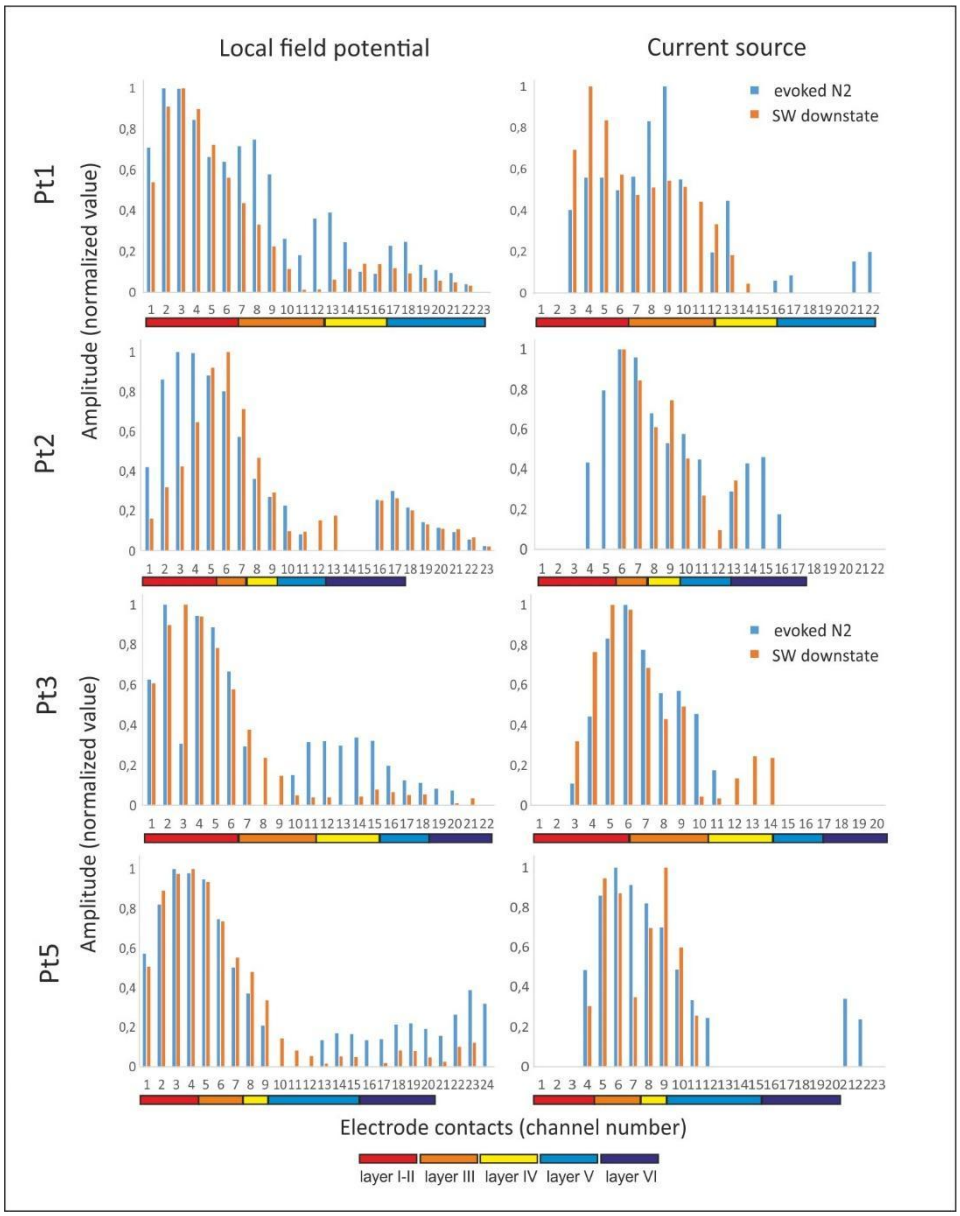

Figure 16. N2 and SWd amplitude patterns across cortical layers (10). Normalized field potential and current source amplitudes for N2 (blue bars) and SWd (orange bars) on each microelectrode in four patients, with layer-specific colors. N2 and SWd show similar intra-cortical patterns, with maximal field potentials in upper layers and current sources predominating in upper and middle layers.

Figure 5e demonstrates the prominent decrease in neural firing during both SWd and N2, corresponding to neural “off ” periods. The temporal association of sSW and N2 is illustrated on the overlaid LFP and CSD plots of Fig. 5f. Despite the slower progression and higher amplitudes of sSWs, the laminar characteristics of N2, described in the previous section, are highly similar to those observed by sSW. To highlight the similarities, the same N2 measures of the same patients were placed by the side of sSW data (Fig. 5, 16). To quantify the above-mentioned similarities in LFP, CSD, MUA and TFR of N2 and sSW, we compared the amplitudes measured on individual channels. In all patients, we found a strong relationship between all parameters: across channels of the superficial negative potential in absolute and normalised amplitude (LFP; Pearson’s r = 0.92 for Pt1), in current source density (CSD; r = 0.75 for Pt1; Pt2 r = 0.76; Pt3 r = 0.88; Pt5 r = 0.878) and in MUA decrements (MUA; r = 0.79 Pt1), while the extent of spectral power decrease correlated weakly (TFR; r = 0.41 Pt1) (Fig. 5 row3, Fig. 6a). There was no significant difference in amplitude between N2 and sSW downstate in either cortical layer, both in terms of field potentials and current sources (two-sample t-tests: layer I-II p = 0.31, layer III p = 0.48, layer IV p = 0.12, layer V p = 0.09, layer VI p = 0.31; bootstrap estimation statistics for each cortical layers) (Fig. 6b, c, n = 4). Maximal amplitudes were measured in supragranular cortical layers (field potential: layer I-II, current source: layer III) for both potentials (Fig. 6b, 16). Amplitude differences between N2 and SWS downstate are illustrated at a Gardner-Altman estimation plot (Fig. 6c). Results of Bayesian Pearson correlation indicated very strong evidence (BF = 86.48) in favour of a positive correlation between N2 and SW downstate amplitude (r = 0.77, median = 0.71, 95% CI [0.39, 0.91]) in layer III. Regarding CSDs, there were strong and extreme evidences of correlation between N2 and SW downstate source amplitude in layerI-II (r = 0.76, 95% CI [0.44, 0.89], BF = 465), layer III (r = 0.68, 95% CI [0.23, 0.86], BF = 15.5), layer IV (r = 0.87, 95% CI [0.49, 0.96], BF = 143) and layer V (r = 0.86, 95% [0.62, 0.95], BF = 6290), suggesting similarities in their laminar distribution (see our paper (10)/ Supplementary Table S4).

DOI:10.14753/SE.2025.3208

V. Discussion

Our findings provide an in-depth examination of layer-specific dynamics in the human neocortex through the analysis of two critical phenomena: sleep spindles and cortico-cortical evoked potentials (CCEPs). By examining these two phenomena with intracranial laminar microelectrode (LME) and electrocorticography (ECoG) recordings, in seven epileptic patients, we explored how each reflects underlying laminar cortical activity, including thalamocortical and cortico-cortical processing. By analyzing these events separately, we elucidated distinct yet complementary roles of cortical layers in supporting both intrinsic oscillatory activities and responses to direct cortical stimulation. We investigated several aspects of sleep spindle characteristics, including co-occurrence patterns, laminar profiles, and also the dynamics of neuronal firing and their relationship to sleep spindle oscillations, in order to reveal functional differences across spindle subtypes (9). We examined the electrophysiological properties of CCEP components and their relationship to sleep slow waves (sSWs), at the levels of local field potentials (LFP), current source density (CSD), multiunit activity (MUA), and single-unit activity (SUA). We observed similarities between the downstate of intrinsic sleep slow waves (SW) and the N2 component of CCEP, supporting our hypothesis that SW-like activity can be elicited even in the awake state (10).

In the analysis of sleep spindles (9), we found that spindles detected in cortical layers are often local events (Fig. 8/C), typically confined to a single cortical layer, and co-occur in other layers in 50-80% of cases, with co-occurrence in the nearest ECoG derivation about one-third of the time (Fig. 9). Larger, higher-amplitude spindles show more frequent co-occurrence with nearby layers. This finding aligns with previous research on the spatial extent and synchronization of sleep spindles, demonstrating that the most localized spindles are captured by intracortical recordings (LME), while larger spindles detected in ECoG are more widespread (14, 30, 31). Our study, however, is the first to extend this finding to a combination of subdural and intracortical electrodes, showing that these co-occurrence patterns are general phenomena. Importantly, LME spindles exhibit highly variable laminar topographies and can occur in any cortical layer, but their laminar profiles are not distinctly associated with spindle subtypes -slow and fast spindles, or spindles with variable cortical involvement (local and global spindles, Fig. 11)-, contrary

to earlier hypotheses suggesting such differences (26, 36). Despite the variable laminar topographies the EEG activity recorded via LME during ECoG spindles is highly stereotypical and shows an amplitude distribution which is very stable at least within the same patient (Fig. 12). These findings align with a model of sleep spindle generation suggesting that spindles may originate from multiple thalamocortical (or potentially cortico-cortical) networks with diverse cortical innervation patterns. Only exceptionally localized spindles—likely undetectable by EEG or ECoG (84, 85)—depend on a single, distinct generator. In contrast, larger spindles typically involve multiple networks, resulting in co-occurrence across multiple layers and producing a more consistent laminar profile. Both slow and fast spindles rely on similar cortical networks, and their laminar profiles do not significantly differ across subtypes. The similar laminar profile of slow and fast spindles is also in line with recent findings showing their similar coupling to thalamic downstates (86), and these findings overall suggest that any functional differences between sleep spindle subtypes are unlikely to be driven by different generating networks. When examining the neuronal dynamics underlying sleep spindles, we replicated previous findings regarding single-unit activity (SUA) and multi-unit activity (MUA), showing that SUA was strongest during sleep spindle troughs and the preferred phase of single-unit discharges was during the positive-negative transition of sleep spindles, with MUA exhibiting an antiphase relationship with local field potentials (LFP) across most cortical layers. Unlike in case of LFPg and CSD, we observed notable differences in the preferred SUA phase angles and the LFPg-MUA relationship across spindle subtypes (but also cortical layers and patients). This suggests that local neuronal events and their contribution to the local field potential are more heterogeneous across sleep spindle subtypes than laminar topography, and may contribute to functional differences. However, due to the lack of consistent effects across the two patients as well as the relatively low statistical power of our study this issue requires further research. Overall, our findings suggest that any differences in spindle subtypes are more likely to be driven by variations in local neuronal activity rather than differences in their laminar profiles (9).

The second part of our study (10) focused on the electrophysiological changes related to various CCEP components on the level of LFP, CSD, multi- and single unit activity, revealing that CCEP responses involve widespread but layer-specific cortical activation.

In particular, single pulse electrical stimulation (SPES) was found to produce significant responses in deep layers associated with cortico-cortical communication pathways, suggesting a prominent role of these layers in mediating evoked responses. Unlike sleep spindles, which are strongly influenced by thalamocortical input, CCEP responses are thought to primarily reflect intracortical and cortico-cortical circuitry, which aligns with our findings of laminar activation patterns that are distinct from those seen in spindles. The laminar specificity observed in CCEPs may also relate to structural properties of these layers, where descending and ascending cortico-cortical fibers terminate, implicating these regions in the integration of evoked information across the cortex. Across patients, we identified similar CCEP components grouped into three categories based on their latency and underlying cortical mechanisms: early (P1, N1), middle (P2, N2), and late (P3) (Fig. 2a). Though distinct latency thresholds were not determined between categories, approximate latency values were as follows: N1 around 20 ms, P2 and N2 approximately 60 ms and 150 ms, respectively, and P3 around 375 ms. The latency of CCEP components remained stable across cortical layers, indicating that separate cortical processes are involved in these phases (Fig. 2d/2). We found that early components (P1, N1) were most reliably evoked from nearby stimulation sites, typically within 1 cm (Fig. 2d/5), while middle and late components exhibited less distance dependence. N1's latency and amplitude, linked to cortico-cortical projections within functional networks, might reflect the proximity and number of tracts between stimulation and response sites (48, 49). N2, however, was not distance-dependent and occurred more frequently than other peaks at all distances, possibly reflecting cross-network activation propagated to subcortical and functionally less connected regions. P2 and P3 were identified in lower rates, similar to N1 peak, while in terms of stimulation distance appeared to lie in-between N1 and N2. P2 was mainly evoked within 1 cm but appeared more consistently at farther stimulation sites compared to N1. In contrast, P3 was more often elicited by stimulations from 3 cm away but remained less frequent than N2. This pattern suggests that P2 and P3 are generated by the weighted contribution of N1 and N2-related processes, respectively (Fig. 2d/5). Additionally, stimulation within or outside of the seizure onset zone (SOZ) did not significantly affect CCEP component appearance, though N1 and P2 were more frequent within the SOZ. Increased short-distance connectivity and excitability in epileptogenic networks, which are suggested to elevate

N1 amplitude, may explain this finding (45). However, the lack of statistical significance could be due to our small sample size, and further research on a larger dataset is warranted. We found a discrepancy between postsynaptic processes (LFP and CSD) and unit firing (MUA and SUA). Most of the CSD components were found in the superficial layers (I-III) while the MUA involved mostly the deep layers shifting upwards to the middle layers. The early components were associated with an alternating sink-source pattern in superficial layers (I-III) starting with a layer III sink under P1 followed by a layer I-II sink during N1. There was also a low amplitude early sink in layer V during P1, as the only deep layer CSD component throughout the whole CCEP pattern. The early MUA response showed a huge increase mostly but not exclusively in the deep layers and wide-band spectral power with maxima in the infragranular layers (Fig. 2c) indicating strong excitation during this phase. Furthermore, the most prominent increase in SUA relative to baseline was found also in lower-middle layers. Layer V neurons have extended dendritic arborization spanning across multiple layers and a widespread projection system, involving both subcortical, intra- and interlaminar connections (87). Therefore, these cells, especially large pyramidal neurons with tufted dendritic arborization in layers I/II, are suitable drivers of stimulation- elicited responses, depolarized either through their dendritic trees or by traversing axons. In the latter case, the impulse conducted by the axons can travel both orthodromically, leading to trans-synaptic neural activation and antidromically, however backpropagation is thought to contribute to stimulation-evoked cortical responses to a lesser degree (37, 71, 88). Hence, P1 most likely corresponds to suprathreshold depolarization of layer V cells. In contrast to P1, N1 is thought to represent oligo- or polysynaptic activation (71). Activation originating in layer V spreads across all cortical layers, with cells forming dense connections in deep layers that sustain infragranular MUA. These cells also extend vertically through prominent axon bundles (87). Consequently, signal propagation primarily follows a vertical trajectory, as confirmed by recent layer-specific microstimulation studies in the rat visual cortex (89), which demonstrated that stimulation in layers V and VI primarily travels along the cortical column (90). Layer V cells densely innervate layers I/II through feedback projections, both directly and via long-range connections involving excitatory neurons in layers III/IV, likely creating a superficial sink linked to N1. Unlike the early components, the middle components presented with

surface-positive (P2) and surface-negative (N2) waves, originating from superficial (layer I-II) and middle (layer III) sources, respectively, and were associated with reduced MUA, SUA, and TFR. This observed neural inhibition may result from both local and long-range inhibitory effects. Animal studies have demonstrated that while layers II/III contain extensive recurrent excitatory circuits that selectively amplify sensory inputs, they also experience greater inhibitory control compared to deeper layers (90). A study on intracortical microstimulation in awake macaque monkeys found that stimulation leads to spiking inhibition, with or without a preceding excitatory response (88). The authors observed that inhibitory responses, unlike excitatory ones, were independent of stimulation distance (up to 4.5 mm) and occurred 5–100 ms after the stimulus. They proposed that inhibition without prior excitation could be due to the activation of long horizontal fibers with stronger feedforward connections to inhibitory neurons than to principal cells, particularly in layer II/III cells. When an excitatory response is triggered, it further activates feedback inhibitory circuits. Our finding that P2 is more likely to be induced from closer stimulation sites (1–2 cm) aligns with the idea that reduced neural activity and superficial source during P2 arise from feedforward/feedback inhibition by local interneurons. Considering the 5–100 ms time frame for neuron spiking suppression after microstimulation (88), this mechanism could contribute to both P2 and N2 components. However, existing literature on CCEPs suggests that the N2 component likely has, at least in part, a subcortical origin (49, 91). The P3 component identified in our data appears as a rebound following N2, characterized by an upper-middle layer sink and a significant increase in MUA and SUA. This activation pattern closely resembles sleep SWs, suggesting a potential involvement of thalamocortical pathways (as discussed later in detail). Based on our findings, the laminar intracortical profile of the sSW downstate and the N2 component of CCEP share notable similarities. The cortical sources of the negative phase of sSW and N2 were located in the supragranular layers (I-III), with peak amplitudes observed in layer II (see Figs. 5, 6b and Fig. 16). During both N2 and sSW, LFP changes showed a negative potential in the upper layers followed by a positive potential in the same layers during P3. Biphasic CSD responses, showing a source in N2 and a sink in P3, were primarily localized to the middle-upper layers (II-IV), indicating activation of the supragranular portion of the cortex after cortical stimulation. Both potentials were associated with broad TFR decreases and increases during N2 and P3,

respectively, mirroring changes seen in sSW (Fig. 5). A typical cortical downstate is marked by neuronal silence, outward currents from neurons in the upper-middle layers, and a decrease in wideband power (7, 92). According to these criteria, we propose that N2 represents a single downstate of an SW cycle. Following N2, the rebound excitation observed in P3 exhibits distinct properties, such as increased neuronal firing, inward currents on the CSD, and an increase in spectral power, which are characteristic of cortical upstates (7, 55, 93, 94). Therefore, we suggest that these components together represent one complete cycle of a sleep slow wave. There is evidence from animal (66) and human cortical electrical (63) and transcranial magnetic stimulation (64, 65) studies that SWs can be triggered during NREM sleep. SWs evoked by microstimulation of rat cortex showed remarkable similarity to sSWs (66). Likewise, it has been found that TMS evoked SWs in human during NREM sleep have similar features and spreading patterns over the scalp to spontaneous ones (64). Additionally, both spontaneous and sensory-evoked K-complexes were shown to share similar intracortical disfacilitation as spontaneous SWs in epileptic patients implanted with laminar microelectrodes (8). Spontaneous local cortical sleep-like phenomena were observed on cortical regional or columnar level in awake state related to sleep pressure in rats (95) and human participants (67), but also linked to attentional lapses in not sleep-deprived human subject (68, 69), supporting that local sleep phenomena might co-occur with awake brain functioning. In turn, there are few and partially contradicting results on whether and in what form SWs can be elicited in the awake state (64, 70). Massimini et al. (64) state that they could not evoke SWs in awake. The difference between these and our results might arise from the non-invasive nature of the recording technique since EEG combined with TMS cannot record the precise local effects of the stimulation. Pigorini et al. (70) were able to trigger SWs in a more activated, low amplitude, ‘wakefulness-like’ phase of sleep, and in few cases, also in the awake state, when evoked potentials were recorded from the vicinity of stimulated electrodes. Nevertheless, they claim that CCEPs triggered in awake generally lack the suppression of high frequencies characteristic to SWs. The discrepancy between this and our result might arise from the more localised nature of this phenomena during wakefulness, captured only by contacts close to stimulation and microelectrodes. Despite these similarities in laminar distribution of cortical generators, sSWs have higher amplitudes and a slower characteristic than the N2-P3 cycle, although it has to be noted

that while the downstate-upstate cycle is indeed slower, the duration of downstate might be comparable to N2 (Fig. 5f) Regarding the amplitude difference, this is in line with previous findings that both sensory (96) and electrically evoked responses are of larger magnitude during NREM sleep, than in awake state. Considering differential durations, sleep SWs typically consist of a 0.3–0.4 Hz cycle with some variance up to 1 Hz in animals (97). Despite this frequency interval for SW, which is broader in humans (0.5–2 Hz (98)), the cortical pattern of short and long cycles were found to be identical (7). Additionally, there is evidence (99) that downstate-upstate durations can be variable even within an oscillatory cycle. Additionally, both animal (95) and human (67) studies showed that extensive use of certain brain areas results not only in increased SW frequency during sleep but also in greater theta power density when awake in the same cortical areas (100). In the work of Vyazovskiy (95), these theta frequency waves, recorded in sleep-deprived, but awake and behaving rats, were related with neuronal OFF periods. It might be possible that the same neural mechanisms manifest with slightly different durations depending on vigilance state. Based on these results, we think that the frequency itself is not characteristic to this type of cortical oscillation, but the laminar distribution reflects more the similarities of the underlying neural processes. The faster frequency of the N2 component of the CCEP may reflect more localised cortical participation after SPES than the widespread involvement in sleep. Similar phenomena can be observed studying cortical slowing associated with pathological processes, where the frequency rather reflects the severity and the volume of the cortical malfunction than the etiology (101). Based on our findings, we developed a hypothetical model to represent the sequence of intracortical activation during SPES-evoked potentials (Fig. 17). Initially, layer V pyramidal neurons are depolarized (P1), generating a local feed-forward excitation (N1) that reaches layers I-II and disrupts local inhibitory processes, contributing to the active inhibition observed in P2. This is followed by a sleep SW-like cycle: a downstate reflecting disfacilitation across all layers (52) (N2), and an upstate (P3). The transition mechanism between the local neuronal processes (early components and P2) and the evoked SW (N2 and P3) remains unknown. We hypothesize that cortical inhibition during P2 may propagate to the thalamus, potentially triggering an SW(102).

DOI:10.14753/SE.2025.3208

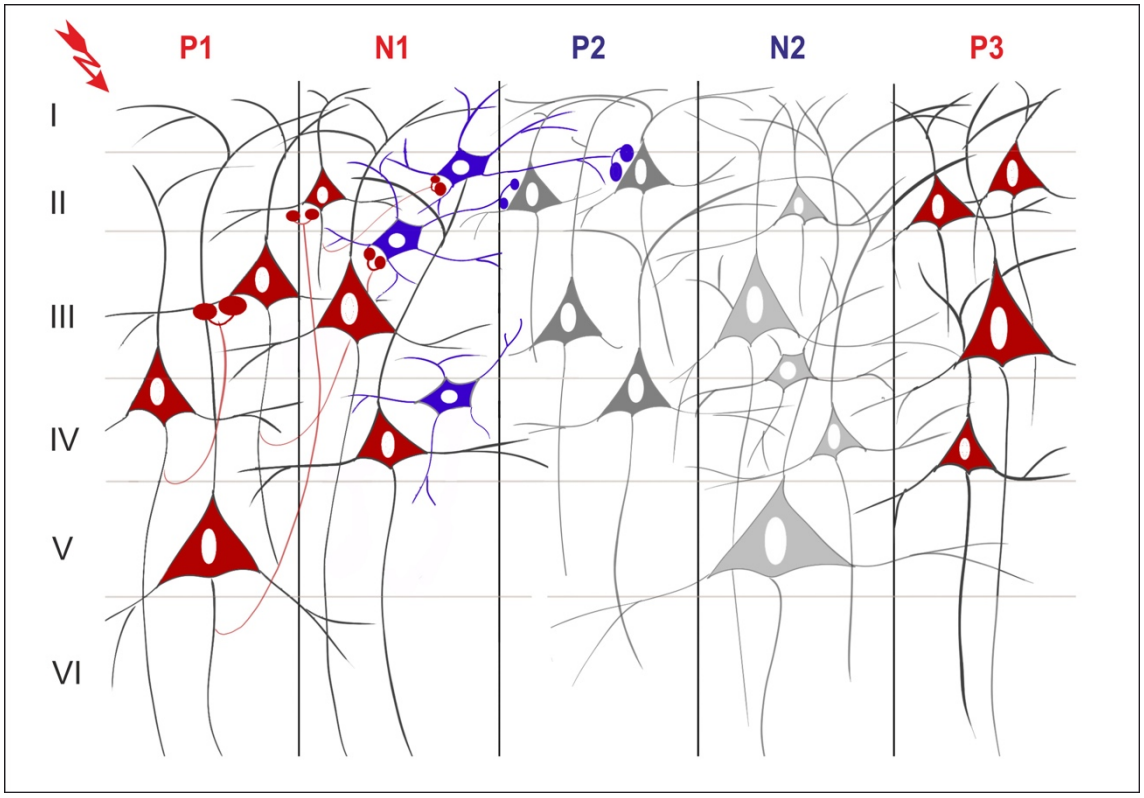

Figure 17. Hypothetical intracortical activation sequence of evoked potentials (10). Based on the laminar profile of CCEPs and single-unit analysis (SUA), electrical stimulation directly activates deep layer pyramidal cells (P1), followed by apical dendritic excitation (N1) via short-range recurrent connections or activation of layer III-IV excitatory neurons. The hyperpolarization and reduced SUA in supragranular layers during P2 may result from a feedback inhibitory mechanism or upper-layer interneuron involvement. The N2 and P3 components represent an evoked sleep slow cycle, with N2 showing a middle layer source and decreased SUA (downstate) and P3 indicating excitation in middle and upper layers (upstate). The transition from P2 to N2 may involve thalamic input. Neuronal firing is represented by red (excitatory) and blue (inhibitory) colors, with synaptic activation shown by colored buttons; gray neurons indicate inactive or inhibited firing.

VI. Conclusions

In conclusion, our study provides novel insights into the spatiotemporal dynamics of sleep spindles and cortico-cortical evoked potentials (CCEPs) in the human neocortex, using a laminar approach with invasive electrophysiology. By analyzing sleep spindle and CCEP responses within intracortical microelectrode (LME) and electrocorticography (ECoG) recordings, we identified unique aspects of layer-specific neural processing. We observed the highly localized nature of LME spindles, their variability across cortical layers, and their relationship to larger, synchronized ECoG spindles. Our findings challenge previous assumptions that spindle subtypes (e.g., slow and fast) correspond to specific laminar profiles, instead suggesting that spindle generation involves overlapping cortical networks, regardless of spindle frequency or spatial extent (9). In our analysis of responses to single-pulse electrical stimulation (SPES), we observed complex intracortical activation sequences, with patterns resembling sleep slow waves (SWs), suggesting that cortical responses in wakefulness may reflect brain mechanisms active during sleep (10). Our hypothetical model proposes an activation sequence where deep layer pyramidal neuron excitation propagates upward, ultimately triggering a downstate-upstate cycle reminiscent of sleep SWs. These results underscore the importance of local cortical dynamics, providing a basis for future studies to explore how these intrinsic and evoked patterns relate to overall brain function across different states of consciousness. Our findings emphasize the complementary roles of distinct cortical layers in sustaining both oscillatory (spindles) and evoked (CCEP) activities, contributing to an enriched understanding of layer-dependent cortical functions. Sleep spindles reflect intrinsic thalamocortical rhythms, while CCEPs offer a window into cortico-cortical connectivity, each supporting unique aspects of cortical processing. These insights have significant implications for neuromodulatory strategies targeting specific cortical layers or pathways, with potential applications for clinical interventions. Our findings may also help to refine stimulation parameters that can be used to induce cortical inhibition. Future research should aim to refine our understanding of these dynamics by using advanced techniques like optogenetics or pharmacological methods to clarify the causal roles of cortical layers in generating spindles and CCEP responses. Expanding this approach to different cortical regions may further reveal whether these patterns are universal or specific to certain areas, ultimately advancing our models of cortical function and plasticity.

DOI:10.14753/SE.2025.3208

VII. Summary

Our study (9, 10) investigates the layer-specific dynamics of sleep spindles and cortico-cortical evoked potentials (CCEPs) in the human neocortex using intracranial laminar microelectrode (LME) and electrocorticography (ECoG) recordings from seven epileptic patients. The goal was to explore how these phenomena reflect thalamocortical and cortico-cortical processing in different cortical layers. Regarding sleep spindles, we found that spindles recorded in cortical layers are often localized events. However, in 50-80% of cases, spindles co-occur across adjacent layers, with larger spindles showing more frequent co-occurrence, and LME-ECoG co-occurrence decreased with greater distance between electrodes. While LME-only spindles were common, most ECoG spindles had corresponding LME spindles. This supports the idea that intracortical spindles are more localized than those detected by ECoG. We did not find distinct laminar profiles for different spindle subtypes (e.g., slow vs. fast spindles), suggesting that any differences between subtypes are more likely driven by local neuronal activity rather than selective contribution of different thalamocortical pathways. Single-unit activity (SUA) peaked during spindle troughs with a phase preference for the positive-negative LFPg transition, while multi-unit activity (MUA) exhibited an antiphase relationship with local field potentials (LFPs), consistent with previous findings. Overall, SUA and MUA were negatively correlated to LFP, with variations by patient, layer, and spindle type, indicating heterogeneous contributions to the local field potential across layers. In the analysis of CCEPs, we identified five major components: early (P1, N1), middle (P2, N2), and late (P3). Based on the laminar profile of CCEPs, we developed a hypothetical model to represent the sequence of intracortical activation during SPES-evoked potentials. Initially, layer V pyramidal neurons are depolarized (P1), creating a local feed-forward excitation (N1) that propagates to layers I-II, where it disrupts local inhibitory processes and contributes to the active inhibition observed in P2. This is followed by a sleep slow wave (SW)-like cycle, with a downstate reflecting widespread disfacilitation across all layers (N2) and an upstate (P3), with increased cell-firing. In conclusion, our research highlights that sleep spindle subtypes are influenced by local neuronal dynamics, not distinct thalamocortical pathways (9). CCEP components involve complex interactions across cortical layers, with late components resembling sleep slow waves, revealing that stimulation can evoke sleep-like cortical dynamics in awake states (10).

VIII. References

1. Nair DR, Burgess R, McIntyre CC, Lüders H. Chronic subdural electrodes in the management of epilepsy. Clinical neurophysiology. 2008;119(1):11-28.
2. Ludwig B, Marsan CA, Van Buren J. Depth and direct cortical recording in seizure disorders of extratemporal origin. Neurology. 1976;26(11):1085-.
3. Talairach J, Bancaud J, Bonis A, Szikla G, Tournoux P. Functional stereotaxic exploration of epilepsy. Confin Neurol. 1962;22(3-5):328-31.
4. Ulbert I, Halgren E, Heit G, Karmos G. Multiple microelectrode-recording system for human intracortical applications. J Neurosci Methods. 2001;106(1):69-79.
5. Ulbert I, Heit G, Madsen J, Karmos G, Halgren E. Laminar analysis of human neocortical interictal spike generation and propagation: current source density and multiunit analysis in vivo. Epilepsia. 2004;45 Suppl 4:48-56.
6. Fabo D, Bokodi V, Szabo JP, Toth E, Salami P, Keller CJ, et al. The role of superficial and deep layers in the generation of high frequency oscillations and interictal epileptiform discharges in the human cortex. Sci Rep. 2023;13(1):9620.
7. Csercsa R, Dombovari B, Fabo D, Wittner L, Eross L, Entz L, et al. Laminar analysis of slow wave activity in humans. Brain. 2010;133(9):2814-29.
8. Cash SS, Halgren E, Dehghani N, Rossetti AO, Thesen T, Wang C, et al. The human K-complex represents an isolated cortical down-state. Science. 2009;324(5930):1084-7.
9. Ujma PP, Hajnal B, Bodizs R, Gombos F, Eross L, Wittner L, et al. The laminar profile of sleep spindles in humans. Neuroimage. 2021;226:117587.
10. Hajnal B, Szabo JP, Toth E, Keller CJ, Wittner L, Mehta AD, et al. Intracortical mechanisms of single pulse electrical stimulation (SPES) evoked excitations and inhibitions in humans. Sci Rep. 2024;14(1):13784.
11. Steriade M. The corticothalamic system in sleep. Front Biosci. 2003;8:d878-99.
12. Fogel SM, Smith CT. The function of the sleep spindle: a physiological index of intelligence and a mechanism for sleep-dependent memory consolidation. Neurosci Biobehav Rev. 2011;35(5):1154-65.
13. Luthi A. Sleep Spindles: Where They Come From, What They Do. Neuroscientist. 2014;20(3):243-56.

14. Andrillon T, Nir Y, Staba RJ, Ferrarelli F, Cirelli C, Tononi G, et al. Sleep spindles in humans: insights from intracranial EEG and unit recordings. J Neurosci. 2011;31(49):17821-34.

15. Born J, Rasch B, Gais S. Sleep to remember. Neuroscientist. 2006;12(5):410-24.

16. Gais S, Molle M, Helms K, Born J. Learning-dependent increases in sleep spindle density. J Neurosci. 2002;22(15):6830-4.

17. Gais S, Born J. Declarative memory consolidation: mechanisms acting during human sleep. Learn Mem. 2004;11(6):679-85.

18. Ujma PP. Sleep spindles and general cognitive ability – A meta-analysis. Sleep Spindles & Cortical Up States. 2021;2(1):1-17.

19. Bodizs R, Gombos F, Kovacs I. Sleep EEG fingerprints reveal accelerated thalamocortical oscillatory dynamics in Williams syndrome. Res Dev Disabil. 2012;33(1):153-64.

20. Ferrarelli F. Sleep in patients with schizophrenia. Curr Sleep Med Rep. 2015;1(2):150-6.

21. Manoach DS, Pan JQ, Purcell SM, Stickgold R. Reduced Sleep Spindles in Schizophrenia: A Treatable Endophenotype That Links Risk Genes to Impaired Cognition? Biol Psychiatry. 2016;80(8):599-608.

22. Gorgoni M, Lauri G, Truglia I, Cordone S, Sarasso S, Scarpelli S, et al. Parietal Fast Sleep Spindle Density Decrease in Alzheimer's Disease and Amnesic Mild Cognitive Impairment. Neural Plast. 2016;2016:8376108.

23. Berencsi A, Bodizs R, Gombos F, Laszlo S, Kovacs I. Sigma frequency dependent motor learning in Williams syndrome. Sci Rep. 2017;7(1):16759.

24. Jones EG. Viewpoint: the core and matrix of thalamic organization. Neuroscience. 1998;85(2):331-45.

25. Jones EG. The thalamic matrix and thalamocortical synchrony. Trends Neurosci. 2001;24(10):595-601.

26. Piantoni G, Halgren E, Cash SS. The Contribution of Thalamocortical Core and Matrix Pathways to Sleep Spindles. Neural Plast. 2016;2016:3024342.

27. Freeman JA, Nicholson C. Experimental optimization of current source-density technique for anuran cerebellum. J Neurophysiol. 1975;38(2):369-82.

28. Spencer WA, Brookhart JM. A STUDY OF SPONTANEOUS SPINDLE WAVES IN SENSORIMOTOR CORTEX OF CAT. Journal of Neurophysiology. 1961;24(1):50-65.

29. Kandel A, Buzsaki G. Cellular-synaptic generation of sleep spindles, spike-and-wave discharges, and evoked thalamocortical responses in the neocortex of the rat. J Neurosci. 1997;17(17):6783-97.

30. Hagler DJ, Jr., Ulbert I, Wittner L, Eross L, Madsen JR, Devinsky O, et al. Heterogeneous Origins of Human Sleep Spindles in Different Cortical Layers. J Neurosci. 2018;38(12):3013-25.

31. Nir Y, Staba RJ, Andrillon T, Vyazovskiy VV, Cirelli C, Fried I, et al. Regional slow waves and spindles in human sleep. Neuron. 2011;70(1):153-69.

32. Piantoni G, Halgren E, Cash SS. Spatiotemporal characteristics of sleep spindles depend on cortical location. Neuroimage. 2017;146:236-45.

33. Bonjean M, Baker T, Bazhenov M, Cash S, Halgren E, Sejnowski T. Interactions between core and matrix thalamocortical projections in human sleep spindle synchronization. J Neurosci. 2012;32(15):5250-63.

34. Ayoub A, Aumann D, Horschelmann A, Kouchekmanesch A, Paul P, Born J, et al. Differential effects on fast and slow spindle activity, and the sleep slow oscillation in humans with carbamazepine and flunarizine to antagonize voltage-dependent Na+ and Ca2+ channel activity. Sleep. 2013;36(6):905-11.

35. Astori S, Luthi A. Synaptic plasticity at intrathalamic connections via CaV3.3 T-type Ca2+ channels and GluN2B-containing NMDA receptors. J Neurosci. 2013;33(2):624-30.

36. Timofeev I, Chauvette S. The spindles: are they still thalamic? Sleep. 2013;36(6):825-6.

37. Entz L, Toth E, Keller CJ, Bickel S, Groppe DM, Fabo D, et al. Evoked effective connectivity of the human neocortex. Hum Brain Mapp. 2014;35(12):5736-53.

38. Valentin A, Alarcon G, Garcia-Seoane JJ, Lacruz ME, Nayak SD, Honavar M, et al. Single-pulse electrical stimulation identifies epileptogenic frontal cortex in the human brain. Neurology. 2005;65(3):426-35.

39. Valentin A, Alarcon G, Honavar M, Garcia Seoane JJ, Selway RP, Polkey CE, et al. Single pulse electrical stimulation for identification of structural abnormalities and

prediction of seizure outcome after epilepsy surgery: a prospective study. Lancet Neurol. 2005;4(11):718-26.

40. Alarcon G, Martinez J, Kerai SV, Lacruz ME, Quiroga RQ, Selway RP, et al. In vivo neuronal firing patterns during human epileptiform discharges replicated by electrical stimulation. Clin Neurophysiol. 2012;123(9):1736-44.

41. Boulogne S, Ryvlin P, Rheims S. Single and paired-pulse electrical stimulation during invasive EEG recordings. Rev Neurol (Paris). 2016;172(3):174-81.

42. Enatsu R, Jin K, Elwan S, Kubota Y, Piao Z, O'Connor T, et al. Correlations between ictal propagation and response to electrical cortical stimulation: a cortico-cortical evoked potential study. Epilepsy Res. 2012;101(1-2):76-87.

43. Yamao Y, Matsumoto R, Kikuchi T, Yoshida K, Kunieda T, Miyamoto S. Intraoperative Brain Mapping by Cortico-Cortical Evoked Potential. Front Hum Neurosci. 2021;15:635453.

44. Yu X, Ding P, Yuan L, Zhang J, Liang S, Zhang S, et al. Cortico-Cortical Evoked Potentials in Children With Tuberous Sclerosis Complex Using Stereo-Electroencephalography. Front Neurol. 2019;10:1093.

45. Zhao C, Liang Y, Li C, Gao R, Wei J, Zuo R, et al. Localization of Epileptogenic Zone Based on Cortico-Cortical Evoked Potential (CCEP): A Feature Extraction and Graph Theory Approach. Front Neuroinform. 2019;13:31.

46. Matsumoto R, Nair DR, LaPresto E, Bingaman W, Shibasaki H, Luders HO. Functional connectivity in human cortical motor system: a cortico-cortical evoked potential study. Brain. 2007;130(Pt 1):181-97.

47. Matsumoto R, Nair DR, LaPresto E, Najm I, Bingaman W, Shibasaki H, et al. Functional connectivity in the human language system: a cortico-cortical evoked potential study. Brain. 2004;127(Pt 10):2316-30.

48. Kunieda T, Yamao Y, Kikuchi T, Matsumoto R. New Approach for Exploring Cerebral Functional Connectivity: Review of Cortico-cortical Evoked Potential. Neurol Med Chir (Tokyo). 2015;55(5):374-82.

49. Veit MJ, Kucyi A, Hu W, Zhang C, Zhao B, Guo Z, et al. Temporal order of signal propagation within and across intrinsic brain networks. Proc Natl Acad Sci U S A. 2021;118(48).

50. Terada K, Umeoka S, Usui N, Baba K, Usui K, Fujitani S, et al. Uneven interhemispheric connections between left and right primary sensori-motor areas. Hum Brain Mapp. 2012;33(1):14-26.

51. Kales A, Rechtschaffen A, University of California LABIS, Network NNI. A Manual of Standardized Terminology, Techniques and Scoring System for Sleep Stages of Human Subjects: Allan Rechtschaffen and Anthony Kales, Editors: U. S. National Institute of Neurological Diseases and Blindness, Neurological Information Network; 1968.

52. Steriade M, Nunez A, Amzica F. A novel slow (< 1 Hz) oscillation of neocortical neurons in vivo: depolarizing and hyperpolarizing components. J Neurosci. 1993;13(8):3252-65.

53. Achermann P, Borbely AA. Low-frequency (< 1 Hz) oscillations in the human sleep electroencephalogram. Neuroscience. 1997;81(1):213-22.

54. Massimini M, Huber R, Ferrarelli F, Hill S, Tononi G. The Sleep Slow Oscillation as a Traveling Wave. The Journal of Neuroscience. 2004;24(31):6862-70.

55. Sanchez-Vives MV, McCormick DA. Cellular and network mechanisms of rhythmic recurrent activity in neocortex. Nat Neurosci. 2000;3(10):1027-34.

56. Sheroziya M, Timofeev I. Global intracellular slow-wave dynamics of the thalamocortical system. J Neurosci. 2014;34(26):8875-93.

57. Fiath R, Kerekes BP, Wittner L, Toth K, Beregszaszi P, Horvath D, et al. Laminar analysis of the slow wave activity in the somatosensory cortex of anesthetized rats. Eur J Neurosci. 2016;44(3):1935-51.

58. Zaforas M, Rosa JM, Alonso-Calvino E, Fernandez-Lopez E, Miguel-Quesada C, Oliviero A, et al. Cortical layer-specific modulation of neuronal activity after sensory deprivation due to spinal cord injury. J Physiol. 2021;599(20):4643-69.

59. Timofeev I, Schoch SF, LeBourgeois MK, Huber R, Riedner BA, Kurth S. Spatio-temporal properties of sleep slow waves and implications for development. Curr Opin Physiol. 2020;15:172-82.

60. Amzica F, Steriade M. Short- and long-range neuronal synchronization of the slow (< 1 Hz) cortical oscillation. J Neurophysiol. 1995;73(1):20-38.

61. Murphy M, Riedner BA, Huber R, Massimini M, Ferrarelli F, Tononi G. Source modeling sleep slow waves. Proceedings of the National Academy of Sciences. 2009;106(5):1608-13.

62. James MK, Joseph TN, Cheryl JD-A, Ping T. Local sleep. Sleep Medicine Reviews. 2019;43:14-21.

63. Marshall L, Helgadottir H, Molle M, Born J. Boosting slow oscillations during sleep potentiates memory. Nature. 2006;444(7119):610-3.

64. Massimini M, Ferrarelli F, Esser SK, Riedner BA, Huber R, Murphy M, et al. Triggering sleep slow waves by transcranial magnetic stimulation. Proc Natl Acad Sci U S A. 2007;104(20):8496-501.

65. Massimini M, Tononi G, Huber R. Slow waves, synaptic plasticity and information processing: insights from transcranial magnetic stimulation and high-density EEG experiments. Eur J Neurosci. 2009;29(9):1761-70.

66. Vyazovskiy VV, Faraguna U, Cirelli C, Tononi G. Triggering slow waves during NREM sleep in the rat by intracortical electrical stimulation: effects of sleep/wake history and background activity. J Neurophysiol. 2009;101(4):1921-31.

67. Hung CS, Sarasso S, Ferrarelli F, Riedner B, Ghilardi MF, Cirelli C, et al. Local experience-dependent changes in the wake EEG after prolonged wakefulness. Sleep. 2013;36(1):59-72.

68. Andrillon T, Burns A, Mackay T, Windt J, Tsuchiya N. Predicting lapses of attention with sleep-like slow waves. Nat Commun. 2021;12(1):3657.

69. Quercia A, Zappasodi F, Committeri G, Ferrara M. Local Use-Dependent Sleep in Wakefulness Links Performance Errors to Learning. Front Hum Neurosci. 2018;12:122.

70. Pigorini A, Sarasso S, Proserpio P, Szymanski C, Arnulfo G, Casarotto S, et al. Bistability breaks-off deterministic responses to intracortical stimulation during non-REM sleep. Neuroimage. 2015;112:105-13.

71. Keller CJ, Honey CJ, Entz L, Bickel S, Groppe DM, Toth E, et al. Corticocortical evoked potentials reveal projectors and integrators in human brain networks. J Neurosci. 2014;34(27):9152-63.

72. Fabo D, Magloczky Z, Wittner L, Pek A, Eross L, Czirjak S, et al. Properties of in vivo interictal spike generation in the human subiculum. Brain. 2008;131(Pt 2):485-99.

73. Ulbert I, Magloczky Z, Eross L, Czirjak S, Vajda J, Bognar L, et al. In vivo laminar electrophysiology co-registered with histology in the hippocampus of patients with temporal lobe epilepsy. Exp Neurol. 2004;187(2):310-8.

74. Wittner L, Henze DA, Zaborszky L, Buzsaki G. Hippocampal CA3 pyramidal cells selectively innervate aspiny interneurons. Eur J Neurosci. 2006;24(5):1286-98.

75. Iber C, Ancoli-Israel S, Chesson A, Quan S. The AASM Manual for the Scoring of Sleep and Associated Events: Rules, Terminology and Technical Specification. 1st ed. Westchester, IL: American Academy of Sleep Medicine; 2007.

76. Bódizs R, Körmendi J, Rigó P, Lázár AS. The individual adjustment method of sleep spindle analysis: Methodological improvements and roots in the fingerprint paradigm. Journal of neuroscience methods. 2009;178(1):205-13.

77. Ujma PP, Gombos F, Genzel L, Konrad BN, Simor P, Steiger A, et al. A comparison of two sleep spindle detection methods based on all night averages: individually adjusted versus fixed frequencies. Frontiers in Human Neuroscience. 2015;9.

78. Delorme A, Makeig S. EEGLAB: an open source toolbox for analysis of single-trial EEG dynamics including independent component analysis. J Neurosci Methods. 2004;134(1):9-21.

79. Nicholson C, Freeman JA. Theory of current source-density analysis and determination of conductivity tensor for anuran cerebellum. J Neurophysiol. 1975;38(2):356-68.

80. Ho J, Tumkaya T, Aryal S, Choi H, Claridge-Chang A. Moving beyond P values: data analysis with estimation graphics. Nat Methods. 2019;16(7):565-6.

81. Hagler DJ, Ulbert I, Wittner L, Erőss L, Madsen JR, Devinsky O, et al. Heterogeneous origins of human sleep spindles in different cortical layers. The Journal of Neuroscience. 2018.

82. Timofeev I, Chauvette S. The Spindles: Are They Still Thalamic? Sleep. 2013;36(6):825-6.

83. Piantoni G, Halgren E, Cash SS. The Contribution of Thalamocortical Core and Matrix Pathways to Sleep Spindles. Neural plasticity. 2016;3024342(10):10.

84. Dehghani N, Cash SS, Rossetti AO, Chen CC, Halgren E. Magnetoencephalography demonstrates multiple asynchronous generators during human sleep spindles. J Neurophysiol. 2010;104(1):179-88.

85. Dehghani N, Cash SS, Halgren E. Emergence of synchronous EEG spindles from asynchronous MEG spindles. Hum Brain Mapp. 2011;32(12):2217-27.

86. Gonzalez CE, Mak-McCully RA, Rosen BQ, Cash SS, Chauvel PY, Bastuji H, et al. Theta Bursts Precede, and Spindles Follow, Cortical and Thalamic Downstates in Human NREM Sleep. J Neurosci. 2018;38(46):9989-10001.

87. Thomson AM, Bannister AP. Interlaminar connections in the neocortex. Cereb Cortex. 2003;13(1):5-14.

88. Yun R, Mishler JH, Perlmutter SI, Rao RPN, Fetz EE. Responses of Cortical Neurons to Intracortical Microstimulation in Awake Primates. eNeuro. 2023;10(4).

89. Allison-Walker T, Hagan MA, Price NSC, Wong YT. Microstimulation-evoked neural responses in visual cortex are depth dependent. Brain Stimul. 2021;14(4):741-50.

90. D'Souza RD, Burkhalter A. A Laminar Organization for Selective Cortico-Cortical Communication. Front Neuroanat. 2017;11:71.

91. Matsumoto R, Kunieda T, Nair D. Single pulse electrical stimulation to probe functional and pathological connectivity in epilepsy. Seizure. 2017;44:27-36.

92. Neske GT. The Slow Oscillation in Cortical and Thalamic Networks: Mechanisms and Functions. Front Neural Circuits. 2015;9:88.

93. Chauvette S, Volgushev M, Timofeev I. Origin of active states in local neocortical networks during slow sleep oscillation. Cereb Cortex. 2010;20(11):2660-74.

94. Sakata S, Harris KD. Laminar structure of spontaneous and sensory-evoked population activity in auditory cortex. Neuron. 2009;64(3):404-18.

95. Vyazovskiy VV, Olcese U, Hanlon EC, Nir Y, Cirelli C, Tononi G. Local sleep in awake rats. Nature. 2011;472(7344):443-7.

96. Rector DM, Topchiy IA, Carter KM, Rojas MJ. Local functional state differences between rat cortical columns. Brain Research. 2005;1047(1):45-55.

97. Steriade M, Nunez A, Amzica F. Intracellular analysis of relations between the slow (< 1 Hz) neocortical oscillation and other sleep rhythms of the electroencephalogram. The Journal of Neuroscience. 1993;13(8):3266-83.

98. Iber C, American Academy of Sleep M. The AASM manual for the scoring of sleep and associated events : rules, terminology and technical specifications. Westchester, IL: American Academy of Sleep Medicine; 2007.

99. Torao-Angosto M, Manasanch A, Mattia M, Sanchez-Vives MV. Up and Down States During Slow Oscillations in Slow-Wave Sleep and Different Levels of Anesthesia. Front Syst Neurosci. 2021;15:609645.

100. Andrillon T, Oudiette D. What is sleep exactly? Global and local modulations of sleep oscillations all around the clock. Neurosci Biobehav Rev. 2023;155:105465.

101. Britton JW, Frey LC, Hopp JL, Korb P, Koubeissi MZ, Lievens WE, et al. In: St. Louis EK, Frey LC, editors. Electroencephalography (EEG): An Introductory Text and Atlas of Normal and Abnormal Findings in Adults, Children, and Infants. Chicago2016.

102. Dossi RC, Nunez A, Steriade M. Electrophysiology of a slow (0.5-4 Hz) intrinsic oscillation of cat thalamocortical neurones in vivo. J Physiol. 1992;447:215-34.

IX. Bibliography of the candidate's publications

IX.1. Publications related to the thesis:

1. Ujma PP, **Hajnal B**, Bodizs R, Gombos F, Eross L, Wittner L, Halgren E, Cash SS, Ulbert I, Fabo D. The laminar profile of sleep spindles in humans. Neuroimage. 2021;226:117587. **(IF:7.4)**

2. **Hajnal B**, Szabo JP, Toth E, Keller CJ, Wittner L, Mehta AD, Erőss L, Ulbert I, Fabo D, Entz L. Intracortical mechanisms of single pulse electrical stimulation (SPES) evoked excitations and inhibitions in humans. Sci Rep. 2024;14(1):13784. **(IF:3.8*)**

Cumulated impact factor of publications related to the thesis: **11.2**

IX.2. Publications not related to the thesis

1. Fabo D, Bokodi V, Szabó JP, Tóth E, Salami P, Keller CJ, **Hajnal B**, Thesen T, Devinsky O, Doyle W, Mehta A, Madsen J, Eskandar E, Erőss L, Ulbert I, Halgren E, Cash SS. The role of superficial and deep layers in the generation of high frequency oscillations and interictal epileptiform discharges in the human cortex. Sci Rep. 2023;13(1):9620. **(IF:3.8)**

2. Benkő Z, Stippinger M, Rehus R, Bencze A, Fabó D, **Hajnal B**, Eröss LG, Telcs A, Somogyvári Z. Manifold-adaptive dimension estimation revisited. PeerJ Comput Sci. 2022;8:e790. **(IF:3.8)**

3. Éltes T, **Hajnal B**, Kamondi A. Concealment of Allergic Reactions to Alteplase by Face Masks in Non-Communicating Acute Stroke Patients: A Warning Call to Improve Our Physical Examination Practices during the COVID-19 Pandemic. Tohoku J Exp Med. 2022;257(2):157-161. **(IF: 2.2)**

4. Hofer KT, Kandrács Á, Tóth K, **Hajnal B**, Bokodi V, Tóth EZ, Erőss L, Entz L, Bagó AG, Fabó D, Ulbert I, Wittner L. Bursting of excitatory cells is linked to

interictal epileptic discharge generation in humans. Sci Rep. 2022;12(1):6280. **(IF: 4.6)**

5. Tóth EZ, Szabó FG, Kandrács Á, Molnár NO, Nagy G, Bagó AG, Erőss L, Fabó D, **Hajnal B**, Rácz B, Wittner L, Ulbert I, Tóth K. Perisomatic Inhibition and Its Relation to Epilepsy and to Synchrony Generation in the Human Neocortex. Int J Mol Sci. 2021;23(1):202. **(IF: 5.6)**

6. Jordán Z, Horváth B, **Hajnal B**, Halász L, Ujvári Á, Fogarasi A, Halász P, Kelemen A, Erőss L, Fabó D. Az epilepsziasebészet eredményességének változása 2006 és 2016 között az Országos Klinikai Idegtudományi Intézetben [Changes of the outcomes of epilepsy surgery within 10 years in the National Institute of Clinical Neurosciences, Hungary]. Orv Hetil. 2021;162(6):219-226. **(IF: 0.707)**

7. File B, Nánási T, Tóth E, Bokodi V, Tóth B, **Hajnal B**, Kardos Z, Entz L, Erőss L, Ulbert I, Fabó D. Reorganization of Large-Scale Functional Networks During Low-Frequency Electrical Stimulation of the Cortical Surface. Int J Neural Syst. 2020;30(3):1950022. **(IF: 5.866)**

8. Huang Y, **Hajnal B**, Entz L, Fabó D, Herrero JL, Mehta AD, Keller CJ. Intracortical Dynamics Underlying Repetitive Stimulation Predicts Changes in Network Connectivity. J Neurosci. 2019;39(31):6122-6135. **(IF: 5.674)**

9. Magyar M, **Hajnal B**, Gyüre T, Ertsey C. Fájdalomcsillapító-túlhasználathoz társuló fejfájás [Medication-overuse headache]. Orv Hetil. 2015;156(30):1195-202. Hungarian. doi: 10.1556/650.2015.30209. PMID: 26186143. **(IF:0.291)**

10. Csépány É, Bozsik G, Kellermann I, **Hajnal B**, Scheidl E, Palásti Á, Tóth M, Gyüre T, Ertsey C. Új önkitöltős migrénszűrő eszköz diagnosztikus hatékonyságának vizsgálata [Examining the diagnostic accuracy of a new migraine screener]. Ideggyogy Sz. 2014;67(7-8):258-68. Hungarian. **(IF:0.386)**

11. Gyüre T, Csépány É, **Hajnal B**, Kellermann I, Balogh E, Nagy Z, Manhalter N, Bozsik G, Ertsey C. The comprehensive headache-related quality of life questionnaire shows significant improvement after withdrawal treatment in medication overuse headache: a pilot study. Ideggyogy Sz. 2014;67(5-6):169-76; discussion 177. **(IF: 0.386)**

Cumulated impact factor of publications not related to the thesis: **33.31**

*Expected IF

DOI:10.14753/SE.2025.3208

X. Acknowledgements

First and foremost, I would like to express my gratitude to Dr. Dániel Fabó for his invaluable guidance and mentorship throughout the course of my PhD. His expertise, encouragement, and support have been instrumental in shaping my research and academic journey.

A special thanks goes to Dr. Johanna Szabó for her hard work and assistance throughout this process over the past couple of years. Her contributions, both professionally and personally, have been immensely appreciated.

I would also like to extend my heartfelt appreciation to Péter Ujma for his expertise and collaboration, which have greatly enhanced my understanding of the field and the depth of our research.

I am deeply thankful to Emília Tóth and Virág Bokodi for their invaluable support, helpful discussions, and also for their help in mastering the research methodology. Their contributions have been crucial in the development of this thesis.

I would like to express my gratitude to Dr. László Entz, Lucia Wittner, István Ulbert and Zoltán Somogyvári for their expertise and insightful perspectives, which have greatly contributed to my understanding of the scientific aspects of my research.

I would like to express my sincere gratitude to my neurosurgeon colleagues, Dr. Loránd Erőss and Dr. László Halász, for their exceptional expertise, collaboration, and unwavering support, which have been invaluable to the success of my research and the realization of this thesis.

I am also grateful to Professor Dr. Anita Kamondi for her kind support over the years. Her perspective and dedication to neuroscience have been a source of inspiration to me.

Finally, I am immensely thankful to the dedicated team of the Epilepsy Monitoring Unit at Semmelweis University, Clinic for Neurosurgery and Neurointervention. Without their help and hard work this research would not have been possible.

I am also thankful to my family, friends, and colleagues who have supported me in countless ways during this journey. Their encouragement and patience have been a constant source of strength.

This thesis would not have been possible without the collective support and contributions of all those mentioned above. I am deeply grateful to each of You.